Effects of pH, ionic strength, and temperature on cesium, barium, cobalt, and europium sorption onto biotite: combined experimental and modelling study

Pawan Kumar*, Stellan Holgersson, and Christian Ekberg

Department of Chemistry and Chemical Engineering, Division of Nuclear Chemistry

Chalmers University of Technology, Kemivägen 4, SE-41296 Göteborg, Sweden

Abstract

The long-term safety of a nuclear waste repository primarily depends on engineered barriers to hinder radionuclide transport via groundwater out to the surrounding bedrock. In case of a barrier fault, the surrounding bedrock serves as the ultimate barrier against radionuclide migration to the biosphere. The Swedish repository for spent nuclear fuel waste is to be built at approximately 500 m depth in a granitic rock formation near Forsmark NPP. The local rock type consists of 3%–12% biotite, a mineral considered to have a considerable sorption capacity for metal contaminants in groundwater. In this study, both batch sorption experiments and modeling were performed to determine the sorption and ion-exchange thermodynamic parameters for four different radioactive elements with biotite. The systematic effects of the pH, ionic strength, and temperature variation on radionuclide sorption were investigated.

The sorption of ^{134}Cs, ^{133}Ba, ^{60}Co, and ^{152}Eu at tracer concentrations (on the order of 10^{-8} M) onto crushed biotite (particle size 0.25–0.5 mm) with an solid to liquid ratio of 1:50 was investigated in batch experiments under inert gas conditions ([O_2] < 1 ppm) for up to two months. The experiments were conducted in triplicate with the pH adjusted to 5, 6, 7, 8, or 9 with pH-buffered solutions containing 0.001, 0.01, and 0.1 M $NaClO_4$ at two temperatures: 40 and 60 °C. The results for pH 5–9 showed that for cesium, barium, cobalt, and europium, at 40 °C and I = 0.001 M, R_d was in the ranges of 0.6–2.3, 0.2–3.8, 0.01–4.0, and 2.4–11.3 m^3/kg, respectively. The corresponding results for 40 °C and I = 0.01 M were R_d = 0.2–0.8, 0.03–5.1, 0.01–10.9, and 0.2–26.9 m^3/kg, and those for 40 °C and I = 0.1 M, R_d = 0.05–0.2, 0.02–0.4, 0.01–8.6, and 2.7–13.9 m^3/kg. For 60 °C and I = 0.001 M, the R_d values for cesium, barium, cobalt, and europium were in the ranges of 0.7–7.8, 0.3–4.4, 0.03–5.7, and 3.1–24.6 m^3/kg,

respectively. The corresponding results for 60 °C and I = 0.01 M were R_d = 0.2–3.2, 0.02–8.1, 0.01–19.3, and 0.2–35.1 m^3/kg, and those for 60 °C and I = 0.1 M were R_d = 0.1–0.6, 0.1–0.8, 0.01–18.0, and 5.3–27.5 m^3/kg.

In addition, titration experiments on solution-suspended biotite were conducted over a pH range of approximately 3–11 at 40 and 60 °C. The results were modelled to obtain $pK_{a,1}$ = –5.0 ±0.2 at 40 °C and –5.3 ±0.2 at 60 °C, as well as $pK_{a,2}$ = –7.0 ±0.3 at 40 °C and –6.9 ±0.2 at 60 °C, using PHREEQC chemical speciation calculations coupled with an error minimization routine.

The sorption of all metals was successfully modelled with a combination of one amphoteric (two pK_a) surface complexation site (≡S) and one ion-exchange site (X). The model was fitted to the data without any compensation for surface electrostatic effects. The modeling results showed that cesium sorption was primarily governed by two surface species: ≡SOCs and CsX. In the case of barium, two surface complexes (≡SOBa$^+$ and ≡SOBaOH) and two ion-exchange species (BaX_2 and BaOHX) mainly contributed to sorption. The cobalt sorption data were modelled using three surface complexes (≡SOCo$^+$, ≡SOCoOH, and $\equiv \mathrm{SOCo(OH)_2^-}$), whereas the europium data were modelled with three surface complexes (≡SOEu^{2+}, ≡SOEuOH$^+$, and ≡SOEu$(OH)_2$) and one ion-exchange species (EuX_3).

The thermodynamic parameters ΔH and ΔS for the sorption reaction were also calculated from the slope and intercept of the linear plot of log K versus 1/T. For surface complexation, the measured increases in the stability constants with T were explained by favorable entropy terms, whereas the negative enthalpy values for the ion-exchange species were calculated to be favorable for the exchange.

Keywords: radionuclide sorption, biotite, surface complex, ion-exchange, sorption modelling, enthalpy, entropy

∗ corresponding author pawank@chalmers.se

1. Introduction

In Sweden, nuclear energy has been part of the energy mix for the last 50 years, and during this time, it has provided stable and CO_2 emission-free electricity to the power grid. The weak point of nuclear power is usually considered to be the high-level radioactive waste (HLW) in the form of spent nuclear fuel that must be addressed due to its high radiotoxicity. Although the novel Generation IV concepts for nuclear power envisage a "closed-end" solution to the waste problem that involves reprocessing and thereby also minimizing the HLW volume, the alternative solution entails of direct disposal of spent nuclear fuel in a final repository and in many countries, including Sweden, is considered to be the most feasible method currently.

The Swedish nuclear fuel and waste management company, SKB, has applied for a license to construct and operate a deep geological nuclear waste repository at the Forsmark area in the municipality of Östhammar on the east coast of Sweden. The repository is designed according to the KBS-3 method, a multi-barrier waste storage concept placed in the granitic rock formation at a level of 400–500 m below surface to store copper canisters with spent nuclear fuel safely for up to 100 000 years (SKBF/KBS, 1983) (SKB, 2010) (Hedin & Olsson, 2016).

In a scenario in which the engineered barriers fail, the granitic rock at the Forsmark site is the last barrier to prevent the migration of radionuclides with groundwater (SKB, 2011). [4]

The radionuclide sorption characteristics of granitic rock and most of the constituent minerals have been extensively investigated. In particular, the Finnish POSIVA and Swedish SKB companies have supported extensive research to determine the empirical values of the distribution coefficient R_d for the sorption of different radionuclides by granitic materials under various conditions (Crawford, 2010) (Hakanen, et al., 2012). In Switzerland, similar studies have been conducted for the Grimsel site. Most results have been released in technical reports, and some have also appeared in academic publications. However, very few studies have been reported that have modelled R_d using mechanistic models, such as surface complexation models (SCMs). Unlike the empirical method of determining R_d, the SCM approach assigns and utilizes specific surface reactions and can thereby provide an understanding of the underlying chemical reactions that govern radionuclide sorption.

The granitic rock at the Forsmark site is composed of many different minerals, including 3%–12% biotite (Drake, et al., 2006) (Selnert, et al., 2008). Biotite is a mineral in the phyllosilicate group and the mica sub-group or family. It is a layered silicate that follows the tetrahedral–octahedral–tetrahedral (TOT) + cation (C) structural pattern. Each tetrahedral layer consists of

Si^{4+} tetrahedrally coordinated to oxygen or hydroxyl groups, whereas the octahedral layer consists of divalent cations, mostly Fe^{2+} and Mg^{2+}. Due to the substitution with Al^{3+} in the tetrahedral layers, each TOT layer has a net negative charge balanced by an additional interlayer of cations with non-hydrated K^{+}, where the latter acts like a glue binding the TOT layers together (Fig. 1-1).

Biotite is considered to have a relatively strong radionuclide sorption capacity compared with those of other minerals present in granite (Tsai, et al., 2009) (Fukushi, et al., 2013) (Tachi, et al., 2015) (Muuri, et al., 2016).

According to a recent literature review of SCM data for radionuclide sorption on granitic minerals, the most commonly used method of performing sorption experiments is the sorption isotherm approach, i.e., varying the radionuclide concentration (Holgersson & Kumar, 2023). This method is suitable for determining values for sorption saturation, where the existence of different sorption sites can be deduced based on the appearance of the sorption isotherm. For example, sorption isotherms have been modelled using a three-site cation-exchange model for the sorption of Cs^{+} (Kyllönen, et al., 2014) and alkaline earths, including radium (Söderlund, et al., 2019). The sorption sites involved in this model were one high-abundance, weakly sorbing planar site; one "intermediate" site at the biotite grain edges; and one low-abundance, strongly sorbing frayed edge site (FES), which is assumed to appear only after considerable weathering of the biotite. The three-site model was originally developed for the clay mineral illite (Bradbury & Baeyens, 2000). At least for Cs^{+} sorption, the identification of one weakly sorbing basal sorption site and one strongly sorbing edge site in biotite is supported by a spectroscopic study (McKinley, et al., 2004).

Sorption isotherm studies usually imply rather high concentrations of the sorbing species. However, to determine the surface reaction constants in SCM, radionuclides must be maintained at tracer levels to prevent the sorbing species from modifying the surface properties of the adsorbent.

According to the same review, systematic studies of sorption on biotite considering several varying parameters, including the pH and ionic strength at the radiotracer level, have seldom been performed (Holgersson & Kumar, 2023). In some studies, the pH has been set to a fixed value and the ion strength has been varied (Söderlund, et al., 2019) or vice versa (Furuya, et al., 1997). Two studies were found in which both the ionic strength and pH were varied while the tracer concentrations of nickel and europium (Puukko, et al., 2007) and europium (Fukushi,

et al., 2013) were fixed. These studies were conducted at room temperature, and the sorption data were modelled either using a combination of one pK_a surface complexation site and one ion-exchange site (Puukko, et al., 2007) or only one ion-exchange site (Fukushi, et al., 2013).

This lack of systematic sorption data for biotite is an unfortunate situation because a broad range of variables should be investigated to develop a robust SCM for a specific mineral (Payne, et al., 2013). In this work, biotite was therefore selected as the first candidate mineral for a specific SCM study. To provide data for SCM to interpret radionuclide sorption onto biotite, the objectives of this work were as follows: (i) to conduct a sorption experiment using four radionuclides (^{134}Cs, ^{133}Ba, ^{60}Co, and ^{152}Eu) on biotite at five pH values (5, 6, 7, 8, and 9) and three ionic strengths (0.001, 0.01, and 0.1 M $NaClO_4$); (ii) to do this at elevated temperatures (40 and 60 °C) to complement our previous data obtained at 25 °C (Kumar et al., submitted manuscript); and (iii) to use PHREEQC geochemical modeling software in conjunction with a PYTHON programming optimization routine to obtain SCM surface complex reaction constants and ion-exchange selectivity coefficients by modelling the measured distribution coefficients.

2. Material and methods

2.1 Material

In this study, a biotite specimen from granitic pegmatite from Risør, Norway was used. In a previous work, the biotite composition was found to be $K_{1.05}(Mg_{0.70}Mn_{0.06}Ti_{0.18}Fe\ (II)_{1.81}Fe\ (III)_{0.25})\ Al_{1.28}Si_{2.62}O_{10}(OH)_2$ (Holgersson, et al., 2024).

The biotite was prepared for the sorption experiments by crushing it with the help of a blender machine with steel knives (M20, IKA) and then sieving it with stainless steel sieves (200 mm ∅ ISO3310-1 type, AS200 sieve shaker, Retsch) to achieve a particle size of 0.25–0.5 mm. The resulting material was then washed several times with 95% ethanol to remove ultrafine particles. The biotite was further dried in a vacuum chamber (Vacucell, MMM) at a temperature of approximately 19±2 °C for several days.

2.2 Mineral characterization

The biotite specimen characterization in terms of specific surface area (SSA), acidic site density (ASD), and cation-exchange capacity (CEC) has been previously reported (Kumar et al., submitted manuscript). The experimentally obtained SSA, ASD and CEC were determined to be 0.47 ±0.01 m^2/g, $3.3 \pm 0.6 \times 10^{-6}$ mol/g and $1.0 \pm 0.1 \times 10^{-5}$ mol/g, respectively.

2.3 Titration on biotite for surface pKa values

Continuous titration on suspensions of biotite in $NaClO_4$ solutions in triplicate was performed to determine the acid-base properties of the biotite mineral at 40 ± 2 °C and 60 ± 2 °C. Standard solutions of 0.01 M HCl and 0.1 M NaOH (both Titrisol, Merck) were used as titrants, where the latter was prepared and stored in an inert gas glovebox (UNILab, MBraun) to avoid carbonate formation in the solution. A closed glass vessel and computer-controlled automatic titration instrument (905 Titrando, Metrohm) were utilized, as well as a glass electrode (6.0250.010, Metrohm). The vessel temperature was maintained via a water recirculation and heating bath (TC120, Grant). Next, 0.5 g of mineral was added to 50 mL of 0.01 M $NaClO_4$ electrolyte solution. The suspension was stirred for 10 min, and ~2.5 mL of HCl solution was added to obtain a pH of approximately 3. The suspension was then titrated with 0.1 M NaOH solution, using a fixed incremental volume of 8 µL/addition in 15 min intervals. Prior to the titrations, the electrode was calibrated by performing the titration procedure proposed by Gran (Gran, 1950). A solid-suspension ratio (S:L) of 1:100 was selected based on the literature

recommendations (Jakobsson, 1999), with the aim of balancing the suspension homogeneity and achieving accurate $\{H^+\}$ measurement.

2.4 Conditioning of biotite into monocationic form

Impurities, such as Ca^{2+} and Mg^+, that are attached to the biotite surface may interfere with batch sorption experiments involving Na^+ electrolytes. Therefore, to minimize the influences of other cations, the biotite was converted into a sodium form, containing only Na^+ on its exchange sites as much as possible. The procedure has been reported elsewhere (Kumar et al., submitted manuscript).

2.5 Batch sorption experiment

Batch sorption experiments were conducted in triplicate at 40 ± 2 **°C** and 60 ± 2 **°C** inside a N_2-filled glove box (UNILab, Mbraun) with an automatic oxygen-removal system ($[O_2] < 1$ ppm). The radioactive tracers used were ^{134}Cs (CsCl in 0.1 M HCl, 10 μg Cs/mL), ^{133}Ba ($BaCl_2$ in 0.1 M HCl, 10 μg Ba/mL), ^{60}Co ($CoCl_2$ in 0.1 M HCl, 10 μg Co/mL), and ^{152}Eu ($EuCl_3$ in 0.5 M HCl, 10 μg Eu/mL) (all provided by Eckert & Ziegler).

Three different concentrations of $NaClO_4$ (Merck, 98%) solutions were prepared: 0.1 M, 0.01 M, and 0.001 M. Each solution was divided into five solutions with different pH values buffered to pH 5–9 using organic pH buffer solutions, as indicated in Table 1, with concentrations of 5 mM for 0.1 M and 0.01 M $NaClO_4$ and 0.5 mM for 0.001 M $NaClO_4$. The buffer solutions were chosen for their negligible tendency to form complexes with metals (Yu, et al., 1997).

Table 1: List of organic buffer solutions used in batch sorption experiments.

Buffer	**pH**
DEPP (1,4-Diethylpiperazine, 98%, Alfa Aesar)	5 and 9
MES (2-(N-Morpholino) ethane sulfonic acid, 99% Sigma-Aldrich)	6
MOPS (3-(N-Morpholino) propane sulfonic acid , 99.5% Sigma-Aldrich)	7
PIPPS (1,4-Piperazine bis-(propane sulfonic acid), 98% Merck)	8

The pH buffered solution was spiked with a mixture of radiotracers (^{134}Cs, ^{133}Ba, ^{60}Co, and ^{152}Eu) at a concentration of approximately 10^{-8} M each; then, the solution pH was re-adjusted using 0.1 M NaOH or $HClO_4$. The pH values were measured with glass electrode and pH meter (pHC 3006-9, pHM 240, Radiometer).

The batch sorption experiment was conducted in 10 mL acid-washed polypropylene centrifuge tubes (Oak Ridge 3119-0010, Thermo Scientific) by adding 0.1 g of crushed biotite together with 5 mL of $NaClO_4$ solution, yielding S:L = 1:50. The batches of biotite were conditioned with neutral 0.001, 0.01, or 0.1 M $NaClO_4$ solutions for one month. Then, the tubes were centrifuged at 45.000g (J2-21 centrifuge with JA20.1 rotor, Beckman) and the supernatants were removed. The solutions were replaced with radiotracer spiked solutions at the five different pH values and placed in heating blocks (Isotemp, Fisherbrand), yielding a total of 90 samples (two temperatures, three ionic strengths, and five pH values, in triplicate). Wall sorption blanks were also prepared, giving an additional 30 tubes without biotite. Acidic blanks (0.1 M HCl) in duplicate were prepared to obtain the reference tracer concentration values.

The sorption experiments were accomplished in approximately two months, where the sampling was conducted in intervals of 2, 14, 28, and 56 days. On each sampling occasion, the tubes were centrifugated at 45,000g and 0.1 mL samples were withdrawn, except on the last occasion, when 0.5 mL samples were withdrawn. The gamma activity of all four radionuclides in the aqueous phase was measured with an HPGe detector equipped with sample changer (GEM23195 detector, 2002C preamp, DSA2000 MCA, GammaAnalyst, Genie2000 v.3.4.1 software, Canberra/Mirion) for 3 h.

Eq.1 was used to compute the radioactivity-based wall sorption-corrected distribution coefficient R_d (m^3/kg) on biotite for each radionuclide (Andersson, et al., 2008):

$$R_d = \left(\frac{\bar{C}\cdot V_{ref}\cdot V_{out,n}}{A_{out,n}} - \left(V_0 - \sum_{i=1}^{n-1} V_{out,i}\right) - L_d - \frac{V_{out,n}\cdot\sum_{i=1}^{n-1} A_{out,1}}{A_{out,n}}\right)\cdot\frac{1}{m} \qquad \text{(Eq.1)}$$

Here, the average measured reference concentration $\bar{C}$ (cpm/L) was obtained from the acidic references; $V_{out,n}$ (L) and $A_{out,n}$ (cpm) are the volume and measured activity of sample n, respectively; V_{ref} (L) is the volume of the radioactive solution that was initially added; V_0(L) is initial liquid volume of the batch, including V_{ref} and any remaining liquid from the preconditioning; m (kg) is the mass of the solid used in the sorption experiment; and L_d (L) is a wall sorption factor measured in the blank series of batch tests. The two summation variables in Eq. 1 were derived from an overall mass balance and were used to adjust for radioactivity and the volumes extracted in the subsequent samplings.

Eq. 2 is essentially the same formula and was used to compute the wall sorption factor; however, because the mass involved in wall sorption is unknown, the wall sorption factor L_d (L) can be defined as

as:

$$R_{d,wall} \cdot m_{wall} = \left(\frac{\bar{C} \cdot V_{ref} \cdot V_{out,n}}{A_{out,n}} - \left(V_0 - \sum_{i=1}^{n-1} V_{out,i} \right) - \frac{V_{out,n} \cdot \sum_{i=1}^{n-1} A_{out,1}}{A_{out,n}} \right) \equiv L_d \qquad \text{(Eq.2)}$$

2.6 Modelling methods for titration and sorption data

The conceptual model used herein to describe sorption on biotite is based on the collected evidence in the literature that at least two distinct types of sorption sites should be present: one on the basal plane surfaces and another at the edges. The conceptualization of the biotite used for modelling is shown in Fig. 2-1.

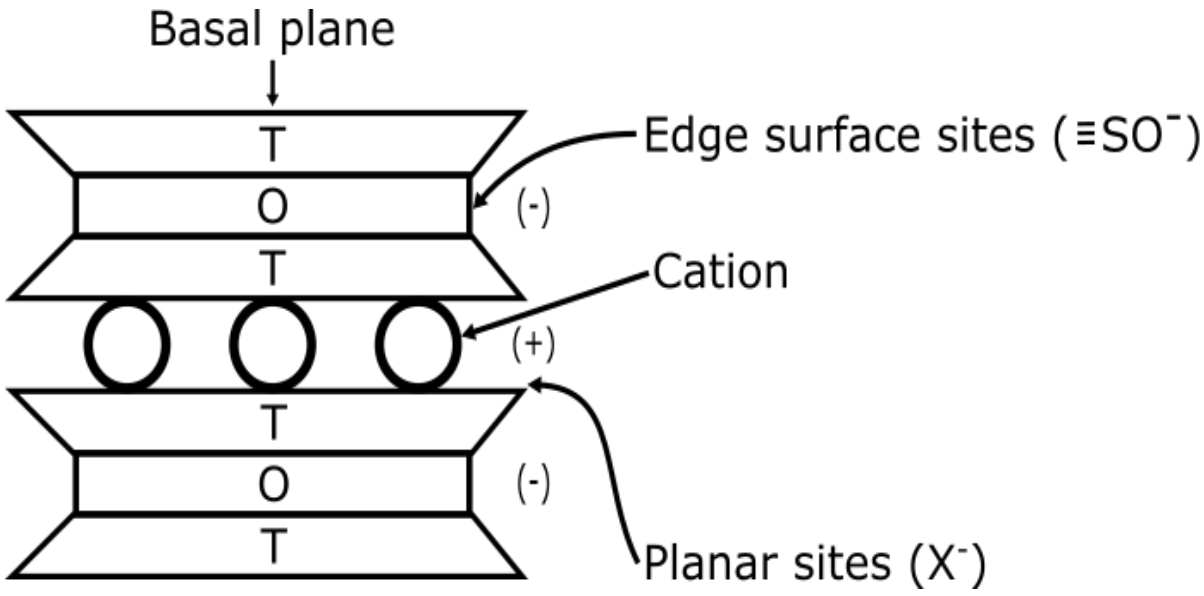

Figure2-1: Graphical representation of the TOT+C structure of the biotite mineral

The basal plane sites are assumed to be ion-exchange sites, denoted as X, and the edge sites are amphoteric surface complexation sites, denoted as ≡SO^-. Thus, any surface charge is only formed at the edges of the mineral, whereas the basal planes are kept neutral by the ion-exchange process. Because the edges of the mineral constitute a relatively small area, below 10% according to one study (Bray, et al., 2015), sorption is not likely to be affected by surface charge, like in the case of metal oxides. Consequently, a non-electrostatic SCM approach was adopted.

The modelled titration data provide information about some basic parameters of the biotite surface, such as the protonation and deprotonation of the amphoteric edge sites and the ion exchange between protons and Na^+. These parameters are combined with the acidic site density (ASD), cation-exchange capacity (CEC), and specific surface site density (SSA), all measured in separate experiments. Together, these parameters provide the total uptake capacity of the surface. Because biotite is an anisotropic mineral and because of the two types of binding sites assumed, the relative SSAs for the different types of sites needed to be modelled. The SSA measured through gas adsorption, and the Brunauer Emmett Teller (BET) evaluation method (Brunauer, et al., 1938) determines the external surface area only and not the interlayer surface areas. However, the CEC can be assumed to measure both the external and interlayer ion-exchange capacities. Thus, the total specific surface area is given by

$$SSA_{tot} = SSA_X + SSA_{\equiv SO^-} = SSA_{X,inner} + SSA_{X,outer} + SSA_{\equiv SO^-} = SSA_{X,inner} + SSA_{BET} \quad \text{(Eq. 3)}$$

In Eq. 3, X denotes ion exchange and $\equiv SO^-$ denotes surface complexation. Note that with this definition, the measured SSA_{BET} is larger than $SSA_{\equiv SO^-}$ but smaller than SSA_{tot}. The relation between the interlayer and outer surface areas depends on the size fraction of the biotite mineral. Therefore, the measured sorption capacities (ASD and CEC), measured per mass biotite, must be used for modelling. However, SSA_{BET} can still be used to calculate the surface-corrected R_d values R_a for comparison with the literature data, if such data are provided along with SSA_{BET}.

The titration data at 40 and 60 ºC were modelled by including the following reactions:

$$NaX + H^+ \rightleftharpoons HX + Na^+ \quad (1)$$

$$\equiv SOH \rightleftharpoons \equiv SO^- + H^+ \quad (2)$$

$$\equiv SOH_2 \rightleftharpoons \equiv SOH + H^+ \quad (3)$$

$$\equiv SO^- + Na^+ \rightleftharpoons \equiv SONa \quad (4)$$

$$\equiv SOH + Na^+ \rightleftharpoons SOHNa^+ \quad (5)$$

The reactions consider ion exchange on the basal planes between the protons and background electrolyte (1), protonation of the edge surface (2 and 3), and strong (4) and weak (5) surface complexes with the background electrolyte. The corresponding selectivity coefficient for ion exchange K_{NaX} is defined by

$$\mathrm{K}_{NaX} = \frac{[HX]\{Na^+\}}{[NaX]\{H^+\}} \quad \text{(Eq. 4)}$$

The surface acidity constants K_{a1} and K_{a2} are defined as

$$\mathrm{K_{a1}} = \frac{[\equiv \mathrm{SOH}]\{\mathrm{H^+}\}}{[\equiv \mathrm{SOH_2}]} \quad \text{(Eq. 5)}$$

$$\mathrm{K_{a2}} = \frac{[\equiv \mathrm{SO^-}]\{\mathrm{H^+}\}}{[\equiv \mathrm{SOH}]} \quad \text{(Eq. 6)}$$

The surface complexation constants for reactions (4) and (5) are

$$\mathrm{K}_{SONa} = \frac{[\equiv \mathrm{SONa}]}{[\equiv \mathrm{SOH}]\{Na^+\}} \quad \text{(Eq. 7)}$$

$$\mathrm{K}_{SOHNa} = \frac{[\equiv \mathrm{SOHNa^+}]}{[\equiv \mathrm{SOH}]\{Na^+\}} \quad \text{(Eq. 8)}$$

where the symbol [] indicates that the concentration is given in units of mol/L.

In the model, any electrostatic effects from possible charge buildup on the mineral surface edges were not considered, which means that a non-electrostatic model (NEM) approach was applied. Reactions similar to (1), (4), and (5) and equations corresponding to Eqs. 4, 7, and 8 were used for the tracer elements.

In the cases of Ba, Co, and Eu, the sorption of hydrolyzed species on the biotite edge sites was also considered. Table 2 shows which hydrolyzed species were used in modelling, along with the corresponding constants β.

Table 2: Hydrolysis constants (log β values) and enthalpies for Ba(II), Co(II), and Eu(III), which were used in sorption modelling, where Z denotes the metal valency

hydroxide complex	Ba(II)[a]	Co(II)[b]	Eu(III)[c]
$Me(OH)^{(Z-1)}$	0.65	4.4	6.4
$Me(OH)_2^{Z-2}$	-	8.2	12.3
$Me(OH)_3^{Z-3}$	-	10.0	17.1

[a] from PHREEQC database MINTEQ, [b] from (Ekberg & Brown, 2016), [c]from (Jordan, et al., 2024)

For the ion-exchange sites on the basal planes, some hydrolyzed species were also considered to participate in an ion-exchange reaction (1). For the species considered, see the Results section.

For the titration data the model was fitted by minimizing the error sum

$$\sum_{i=1}^{n} abs(\{H^+\}_{exp,i} - \{H^+\}_{calc,i}) \quad \text{(Eq.9)}$$

In Eq. 9, n is the number of steps in the titration curve, $\{H^+\}_{exp,i}$ is the measured proton activity at point i, and $\{H^+\}_{calc,i}$ is the proton activity calculated according to the mass balances:

$$\frac{V_{HCl} \cdot C_{HCl} - V_{NaOH} \cdot C_{NaOH}}{V_{tot,i}} = [H^+] - [OH^-] + [HX] + [\equiv SOH] + 2\cdot[\equiv SOH_2] - [\equiv SO^-] - [NaX] \quad \text{(Eq.10)}$$

$$\frac{CEC \cdot m_{biotite}}{V_{tot,i}} = [HX] + [NaX] \quad \text{(Eq.11)}$$

$$\frac{ASD \cdot m_{biotite}}{V_{tot,i}} = [\equiv SO^-] + [\equiv SOH] + [\equiv SOH_2] + [\equiv SONa] + [\equiv SOHNa^+] \quad \text{(Eq. 12)}$$

$$\frac{[Na^+]_{NaClO4} \cdot V_{NaClO4} + [Na^+]_{NaOH} \cdot V_{NaOH,i}}{V_{tot,i}} = [Na^+] + [NaX] + [\equiv SONa] + [\equiv SOHNa^+] \quad \text{(Eq.13)}$$

Here CEC and ASD are the measured cation exchange capacity and acidic site density in moles/g, respectively. $m_{biotite}$ is the mass of biotite in the titration and $V_{tot,i}$ is the total volume at titration point i.

The equation system with the four "master species" H^+, Na^+, HX, and $\equiv SO^-$ was solved for each titration point using PHREEQC software (Parkhurst & Appelo, 2021). The initial contributions of H^+ and Na^+ from the biotite itself to Eqs. 10 and 13, respectively, were judged to be negligible compared with the amounts added as solutions at the start of titration.

The optimization of the model was accomplished by coupling the PHREEQC chemical speciation software with a PYTHON optimization routine through an integration code (Charlton & Parkhurst, 2011) (Wissmeier & Barry, 2011). This code is a Microsoft component object model (COM) version of PHREEQC called IPHREEQC and facilitates a link to communicate and interchange the data between PHREEQC and other software such as Excel and MATLAB and programming languages such as PYTHON and Visual Basic. The optimization parameters are the assumed reaction constants and partitioning coefficients, as defined in Eqs. 4–8. One may also note that these are treated in PHREEQC as valid at zero ionic strength and that activity coefficients are applied to all dissolved species by the program, according to the given ionic strength.

With several parameters, that is, the equilibrium constants in Eqs. 4–8, fixed by titration, a similar model was fitted to the measured distribution coefficients R_d at five different pH values, where the fitting was carried out in triplicate, which gave 15 measured points for the optimization at a fixed ion strength and temperature.

The sorption model also includes a mass balance for the radiotracer element, giving a fifth "master species." Although the batch experiments were conducted with radionuclide mixtures, each radiotracer element was modelled individually. The low radiotracer concentration ($\sim 10^{-8}$ M) was assumed to prevent any potential influences between the radiotracers in their individual sorption behaviors.

A solubility product for biotite could not be found in the literature. Because annite is an end member in the same solid solution series of micas that includes biotite, annite was used as a substitute for biotite and was allowed to be in equilibrium with the solution to simulate any effect of biotite dissolution. The MINTEQ thermodynamic database associated with PHREEQC was used to model the sorption data.

3. Results and Discussion

3.1. Titration modelling results

The biotite titration results at 40 and 60 ºC are shown in Fig. 3-1, and the corresponding optimized reaction constants for biotite are listed in Table 3.

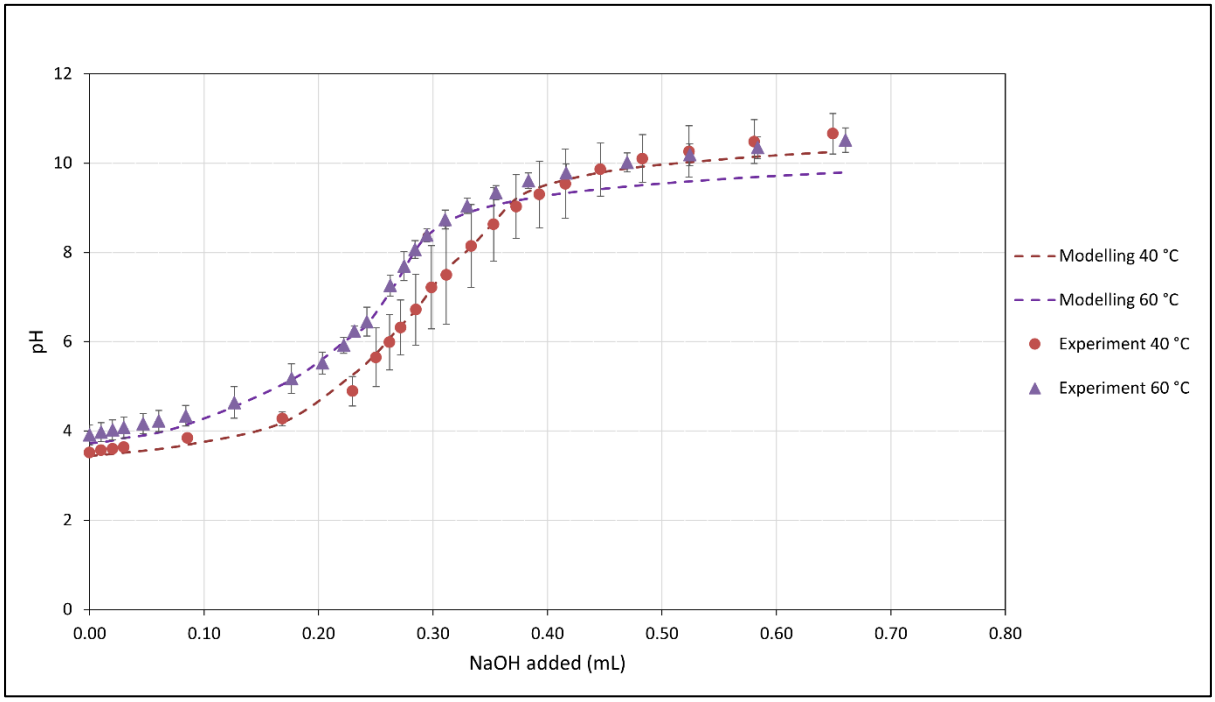

Figure 3-1: Experimental (average of triplicates) and modelled titration curves for a suspension of biotite in 0.01 M $NaClO_4$ solution at 40 and 60 °C.

Table 3: Optimized acidity (≡ SOH_2, ≡ SO^-), cation-exchange (X), sodium inner (≡ SONa), and sodium outer (≡ $SOHNa^+$) sphere complex reactions and their associated reaction constants or coefficients for biotite at zero ionic strength

Reactions	**Constant or coefficient at 40 ºC**	**Constant or coefficient at 60 ºC**
$\equiv \mathbf{SOH_2} \rightleftharpoons \equiv \mathbf{SOH} + \mathbf{H^+}$	−5.0 ±0.2	−5.3 ±0.1
$\equiv \mathbf{SOH} \rightleftharpoons \equiv \mathbf{SO^-} + \mathbf{H^+}$	−7.0 ±0.3	−6.9 ±0.2
$\equiv \boldsymbol{SO^-} + \mathbf{Na^+} \rightleftharpoons \equiv \mathbf{SONa}$	2.0 ±0.4	3.2 ±0.1
$\equiv \mathbf{SOH} + \mathbf{Na^+} \rightleftharpoons \equiv \mathbf{SOHNa^+}$	2.0 ±0.8	2.3 ±0.2
$\boldsymbol{NaX} + \boldsymbol{H^+} \rightleftharpoons \boldsymbol{HX} + \boldsymbol{Na^+}$	2.9 ±0.2	2.9 ±0.1

The changes in pK_a with temperature indicate that the predominant domain of the non-charged ≡SOH surface species becomes narrower with increasing temperature. The increase in temperature therefore seems to favor the charged surface species $\equiv SO^-$ and $\equiv SOH_2^+$.

The stability constants for the Na^+ surface complex appear to increase with increasing temperature, which means that Na^+ sorption on sites of this type is favored by increased temperature. Ion exchange between H^+ and Na^+, on the other hand, seems not to be affected by temperature.

Fig. 3-2 shows the net amount of protons consumed as a function of pH at 40 and 60 ºC. The point of zero surface charge, or pH_{pzc}, is the intersection of the potentiometric titration curves at both temperatures, indicating the absence of charge on the mineral surface. Similar pH_{pzc} results have been reported for biotite (Puukko, et al., 2007).

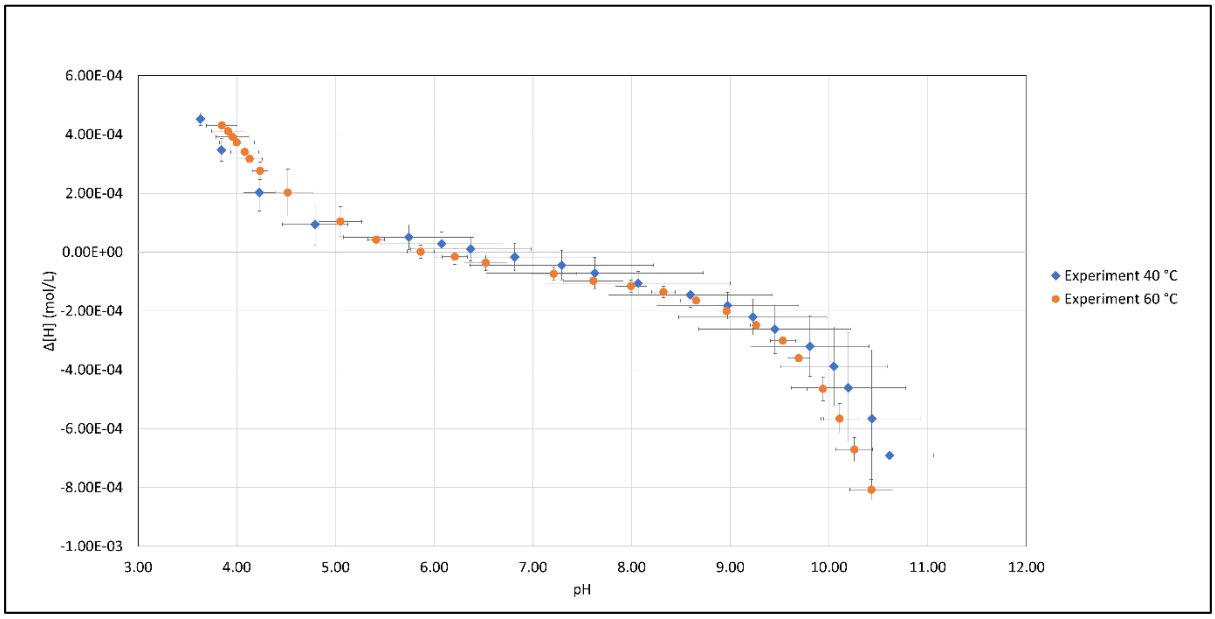

Figure 3-2: Potentiometric titration (average of triplicates) of a biotite suspension in 0.01 M $NaClO_4$ solution at 40 and 60 °C.

The experimental CEC and ASD values was adjusted slightly in order to attain an optimal fit of the titration data, because the experimental values of CEC and ASD were obtained for experiments running for two months, whereas titration experiments typically run for half a day. The biotite samples are not expected to be penetrated with NaOH solution completely, nor are the inner surfaces expected to be in complete equilibrium with the solution at each titration point. The optimized values are shown in Table 4.

Table 4: Experimental and optimized CEC and ASD values.

	Experimental value (mol/g)	Optimized value (mol/g)
CEC	$1.0 \pm 0.1 \times 10^{-5}$	$2.6 \pm 0.5 \times 10^{-5}$
ASD	$3.3 \pm 0.6 \times 10^{-6}$	$1.7 \pm 0.1 \times 10^{-5}$

3.2. Sorption results

The batch sorption experiments lasted for approximately two months. During this time, the apparent R_d values were expected to increase gradually due to an in-diffusion transport process in the biotite grains.

The time-dependent results were comparable for all radiotracers. Therefore, for illustration purposes, only the time-dependent sorption of barium and cobalt at 0.01 M ionic strength at 25 (Kumar et al, submitted manuscript), 40, and 60 °C is presented in Fig. 3-3. The complete set of time-dependent data for R_d is given in Appendix A in Section A1 (Cs) and A2 (Ba), Tables A3 (Co) and A4 (Eu).

The results indicate that the equilibrium for radionuclide sorption was achieved within one month, after which no significant increase in sorption was observed, but rather a slight decrease. The latter may be an effect of partial dissolution of the biotite surface. The rapid increase in sorption during the first month of the batch experiment may be an indication of the presence of a large number of active sites on the biotite surface. Interestingly, the temperature did not seem to have much effect on the time required to reach equilibrium.

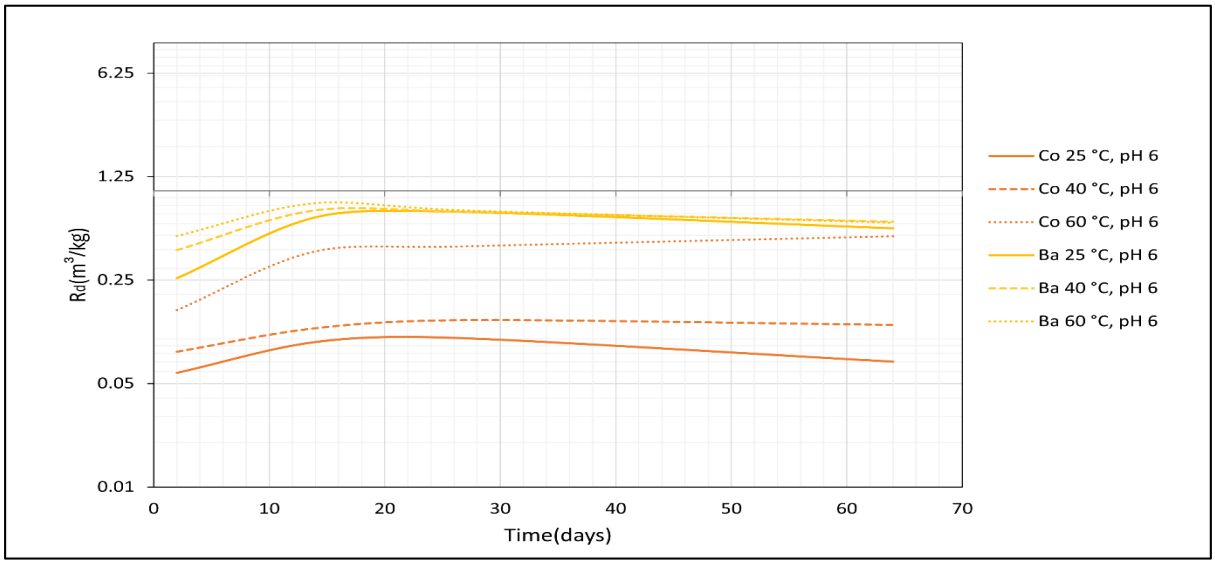

Figure 3-3: Example of the effects of contact time on barium and cobalt sorption onto treated biotite for pH 6 in 0.01 M $NaClO_4$ at 25 (kumar et al, submitted manuscript), 40, and 60 °C

Fig. 3-3 also demonstrates that the temperature has a large positive effect on the sorption of cobalt, but almost no effect on the sorption of barium.

3.3 Sorption modelling results of cesium at 40 and 60 °C

The experimental results for cesium sorption on biotite indicate that all three variables investigated (the ionic strength, pH, and temperature) had significant impacts on the results (see the tables in Appendix A). The final results at two months for 0.001 M are shown in Figs. 3-4 (40 °C) and 3-5 (60 °C).

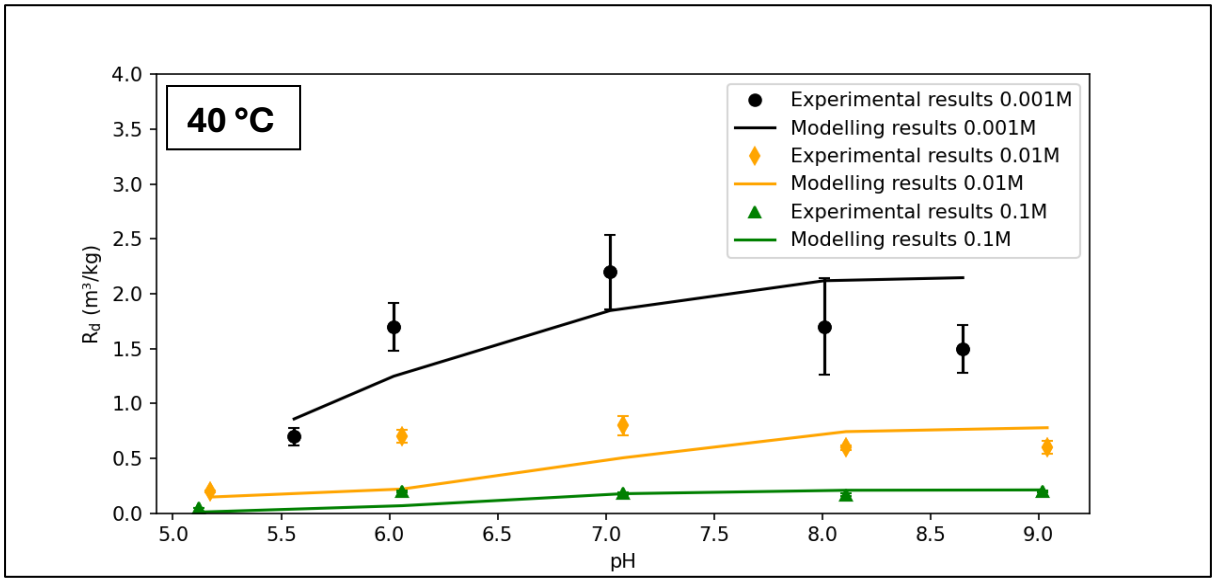

Figure 3-4: Cesium sorption onto biotite mineral in 0.001, 0.01, and 0.1 M $NaClO_4$ solution as a function of pH at 40 °C: measurements (symbols) and modelling results (continuous lines)

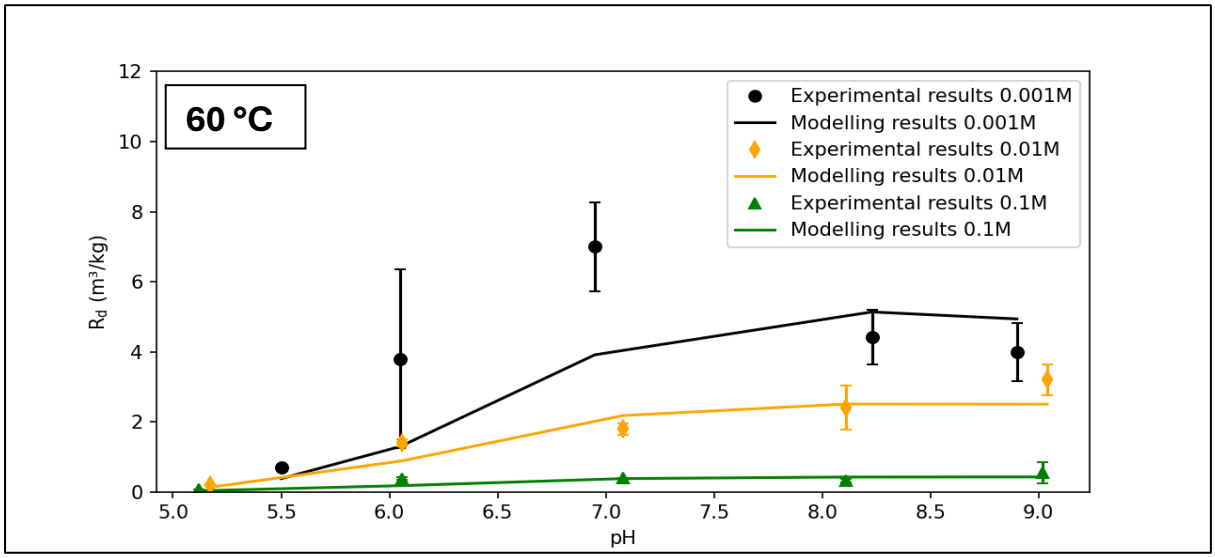

Figure 3-5: Cesium sorption onto biotite mineral in 0.001, 0.01, and 0.1 M $NaClO_4$ solution as a function of pH at 60 °C: measurements (symbols) and modelling results (continuous lines)

At both temperatures, the R_d values of cesium decrease as the ionic strength increases from 0.001 to 0.1 M, which is most likely an effect of the Na^+ ions competing for the accessible sorption sites.

In addition, the effect of pH variation on the R_d values of cesium generally increases with increasing pH at both temperatures. The apparent slight decrease in sorption at 0.001 M ionic strength and temperatures of 40 and 60 °C when the pH increases from 7 to 9 (Figs. 3-4 and 3-5) is probably within the error margin.

The temperature has a relatively large positive effect on cesium sorption, with R_d increasing from 2.3 to 7.8 m^3/kg at 0.001 M. For the two higher ionic strengths, the increases in R_d are lesser but still detectable. The temperature effect is the most pronounced for 0.001 M $NaClO_4$ in the pH range of 7–9. One can therefore expect that the surface species that govern cesium sorption under these specific conditions are also responsible for this temperature effect.

The model for cesium enables the following surface species to form: CsX (ion exchange), ≡SOCs ("strong" complex), and ≡SOHCs$^+$ ("weak" complex). However, only the former two have any effect on the modelling results. Figs. 3-6 (40 °C) and 3-7 (60 °C) display the results of cesium sorption modeling for 0.001 M $NaClO_4$, and the results for 0.01 and 0.1 M are shown in Appendix B.

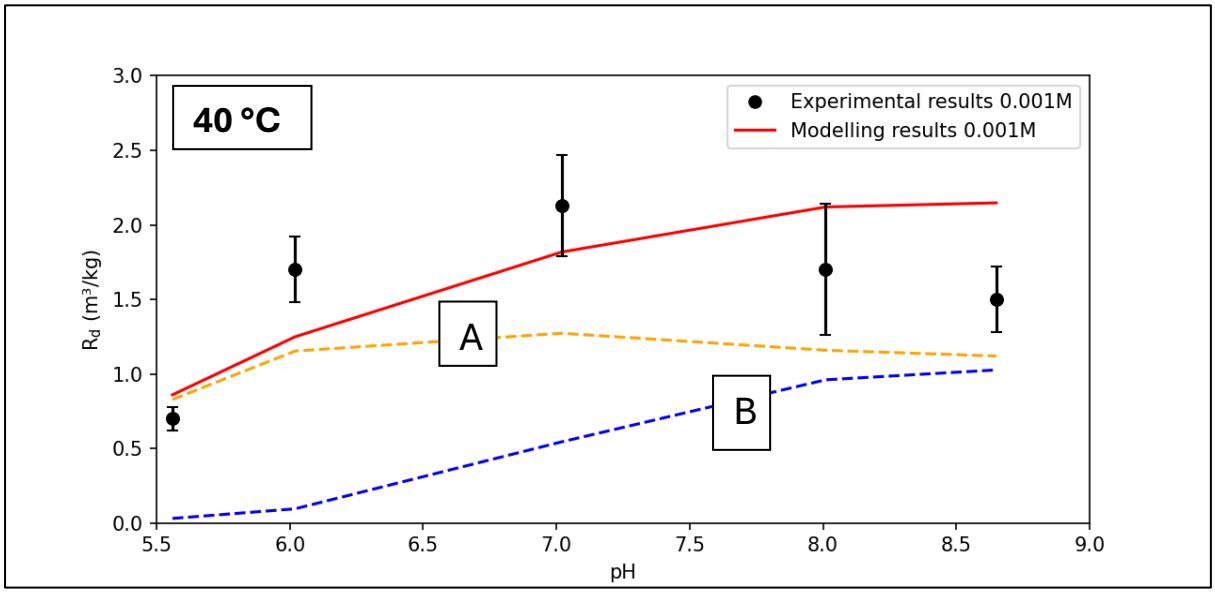

Figure 3-6: Results for cesium sorption onto biotite mineral in 0.001 M $NaClO_4$ solution at 40 ºC (measurements (symbols) and modelling results (continuous lines)), where the contributions of different Cs(I) species to cesium sorption are represented by different curves: (A: yellow line) CsX; (B: blue line) ≡SOCs

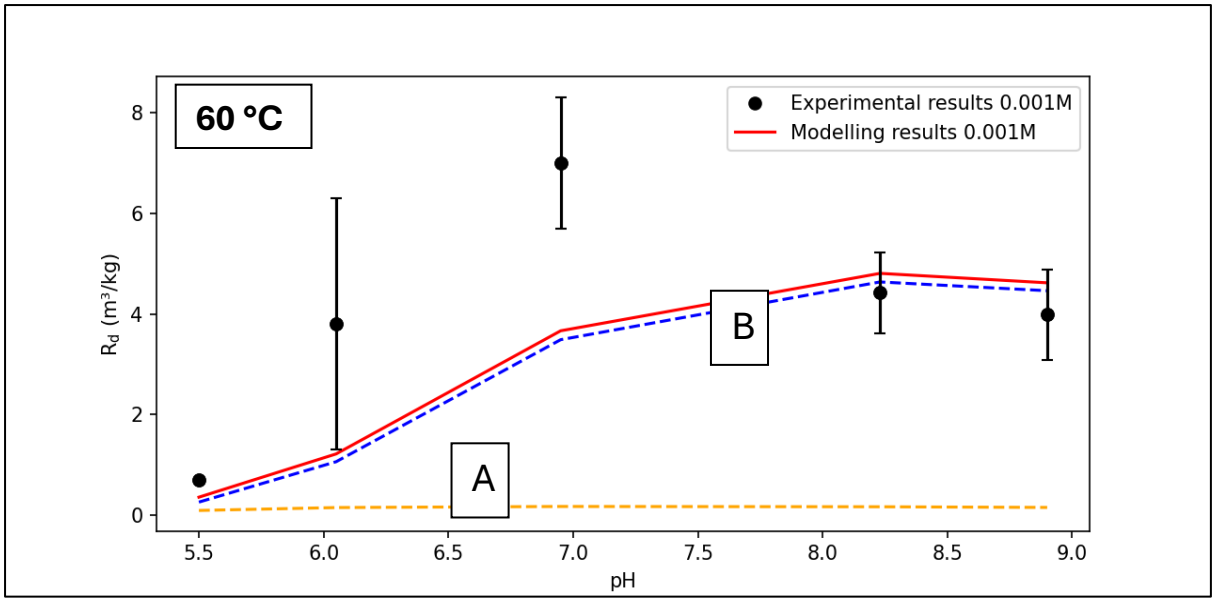

Figure 3-7: Results for cesium sorption onto biotite mineral in 0.001 M $NaClO_4$ solution at 60 ºC (measurements (symbols) and modelling results (continuous lines)), where the contributions of different Cs(I) species to cesium sorption are represented by different curves: (A: yellow line): CsX, (B: blue line) ≡SOCs.

One ion-exchange (CsX) and one surface complexation (≡SOCs) species were sufficient to simulate the cesium sorption data, and the latter surface species seems to be favored greatly by the increase in temperature. The effect is less pronounced at higher ionic strengths due to the competition for surface sites from Na^+.

Additionally, at both temperatures, surface complexation becomes the most significant sorption species as the ionic strength increases from 0.001 M to 0.1 M. The ion-exchange species makes a very low (at 40 °C and pH > 6) to negligible (at 60 °C and pH > 5) contribution to the ion-exchange species, especially at the highest $NaClO_4$ concentration (0.1 M). A summary of the surface reactions used in modelling is given in Table 5.

Table 5: Surface complexation and cation-exchange reactions and their associated constants (log k) for Cs(I) at 40 and 60 °C at zero ionic strength

Reactions		**Log k (40 °C)**	**Log k (60 °C)**
$\equiv SO^- + Cs^+ \leftrightarrow \equiv SOCs$		5.0 ± 0.2	6.2 ± 0.2
$\equiv SOH + Cs^+ \leftrightarrow \equiv SOHCs^+$		Not significant*	Not significant*
Reaction/ (experimental ionic strength) at 40 °C	**Log k (0.001M)**	**Log k (0.01M)**	**Log k (0.1M)**
$Cs^+ + NaX \leftrightarrow CsX + Na^+$	1.8	1.7	1.0
Reaction/(experimental ionic strength) at 60 °C			

$Cs^+ + NaX \leftrightarrow CsX + Na^+$	0.9	1.0	0.8

*The surface complex did not improve the fitting of the model

Table 5 demonstrates that the selectivity coefficients for cation exchange were allowed to vary across the three series of different ionic strengths. This variation was allowed because several previous studies have shown that the selectivity coefficient seems to be dependent on the ionic strength. However, the results presented here indicate that this dependence is not present because the average ion-exchange log k values are 1.5±0.4 (40 °C) and 0.9±0.1 (60 °C), that is, the standard deviations are acceptable.

In conclusion, Cs^+ sorption increased with temperature, especially at low ionic strength at which the competition from Na^+ was low. This effect was ascribed to the formation of the surface complex ≡SOCs. Further, as the temperature increased, surface complexation started to take over as the main sorption process, and at the highest temperature of 60 ºC, ion exchange had a very small role in Cs^+ uptake. Besides the temperature effects, both an increased ionic strength and a decreased pH seemed to suppress Cs^+ sorption by Na^+ and H^+ competition mechanisms, respectively.

3.4 Sorption modelling results for barium at 40 and 60 °C

The experimental and modeling results for barium sorption onto biotite for three ionic strengths and five pH values at 40 ºC and 60 °C are presented in Figs. 3-8 and 3-9, respectively. The complete set of data is shown in the tables in Appendix A. At both temperatures, the R_d values of barium are considerably reduced by the increased ionic strength, a behavior similar to that observed for cesium and a result of increased Na^+ competition for the sorption sites.

In addition, the barium sorption data clearly indicate that the pH has a significant impact on sorption, as shown in Figs. 3-8 and 3-9. The sorption of barium increases continuously up to pH 9, even though this behavior is suppressed at the highest ionic strength. On the other hand, the increase in temperature has little effect on barium sorption, which is evident when comparing Figs. 3-8 and 3-9.

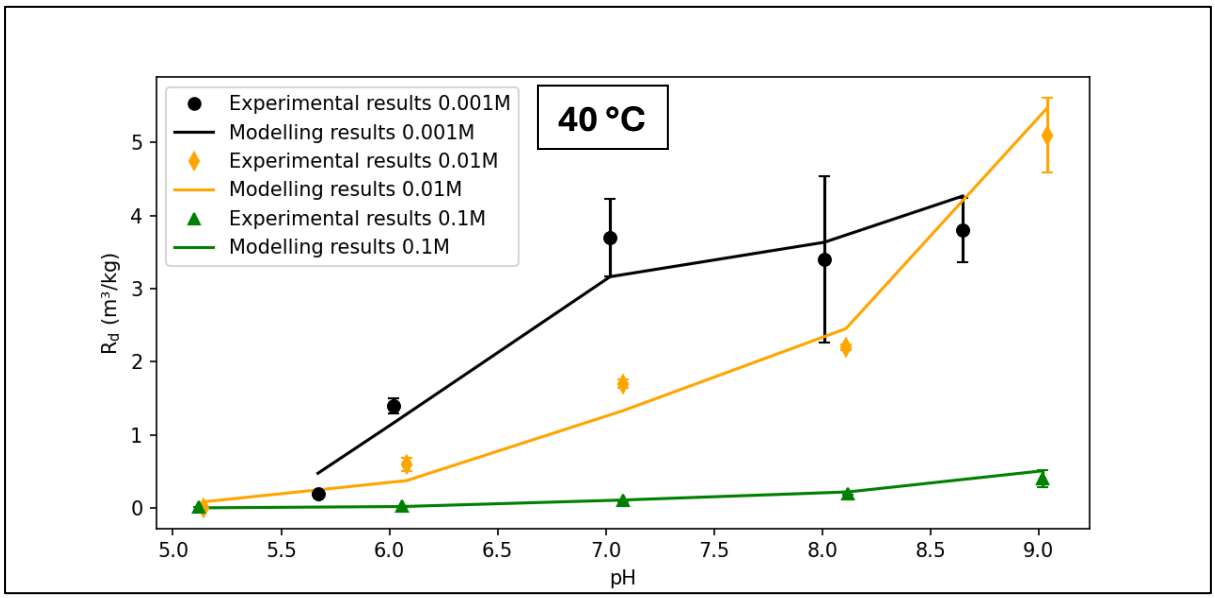

Figure 3-8: Barium sorption onto biotite mineral in 0.001, 0.01, and 0.1 M $NaClO_4$ solution as a function of pH at 40 °C: measurements (symbols) and modelling results (continuous lines).

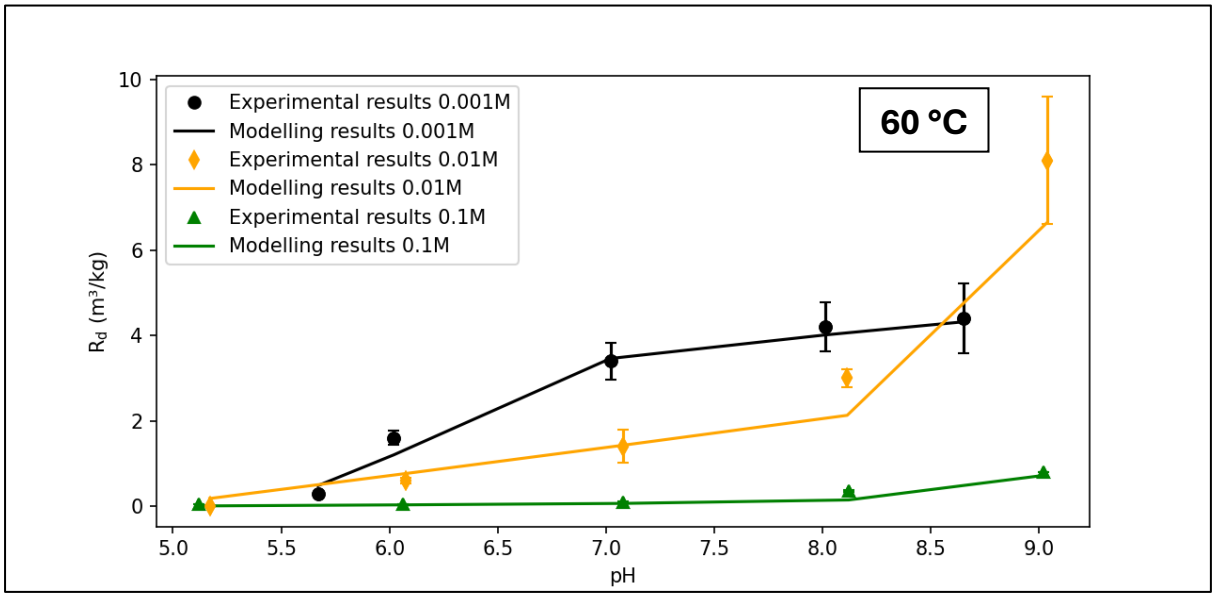

Figure 3-9: Barium sorption onto biotite mineral in 0.001, 0.01, and 0.1 M $NaClO_4$ solution as a function of pH at 60 °C: measurements (symbols) and modelling results (continuous lines)

The barium sorption model initially allows the following surface species to form: BaX_2 and ≡XBaOH (ion-exchange), $≡SOBa^+$ ("strong" complex), $≡SOHBa^{2+}$ ("weak" complex), and the hydrolyzed sorption species ≡SOBaOH. The "weak" complex was subsequently removed from the model because it did not improve the fitting of the model to the data.

Figs. 3-10 (40 °C) and 3-11 (60 °C) display the modeling results for 0.001 M $NaClO_4$, and the results for 0.01 and 0.1 M are shown in Appendix B.

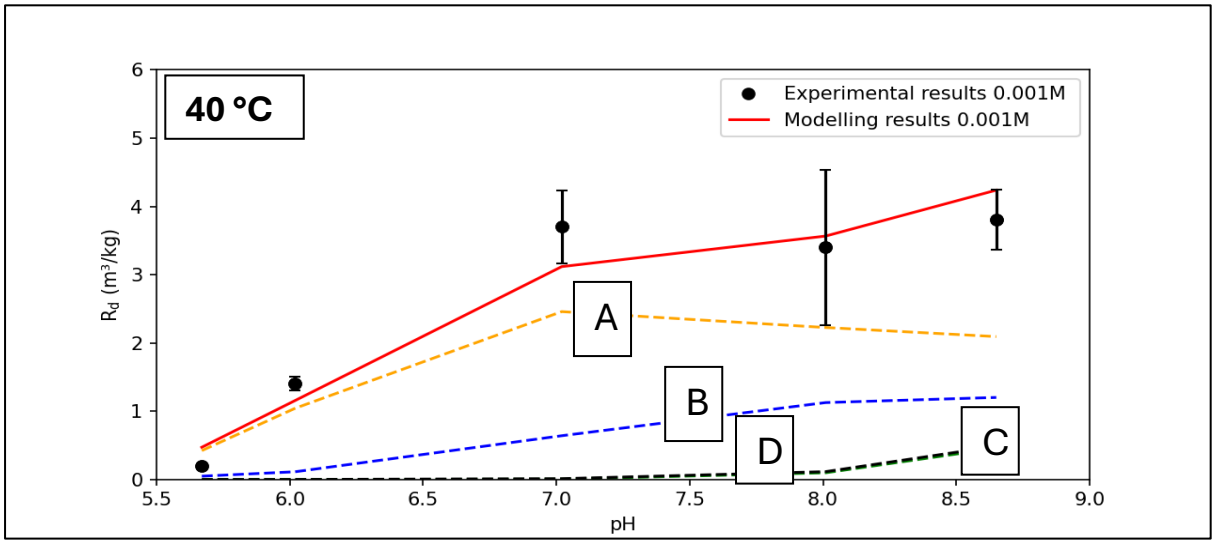

Figure 3-10: Results for barium sorption onto biotite mineral in 0.001 M $NaClO_4$ solution at 40 ºC (measurements (symbols) and modelling results (continuous lines)), where the contributions of different Ba(II) species to its sorption are represented by different curves: (A: yellow line) BaX_2; (B: blue line) ≡SOBa^+; (C: green line) ≡SOBaOH; (D: black line) XBaOH

The contributions of the hydrolyzed species ≡XBaOH and ≡SOBaOH are only evident at pH 8–9. A summary of the exchange reactions employed and their associated selectivity coefficients is given in Table 6.

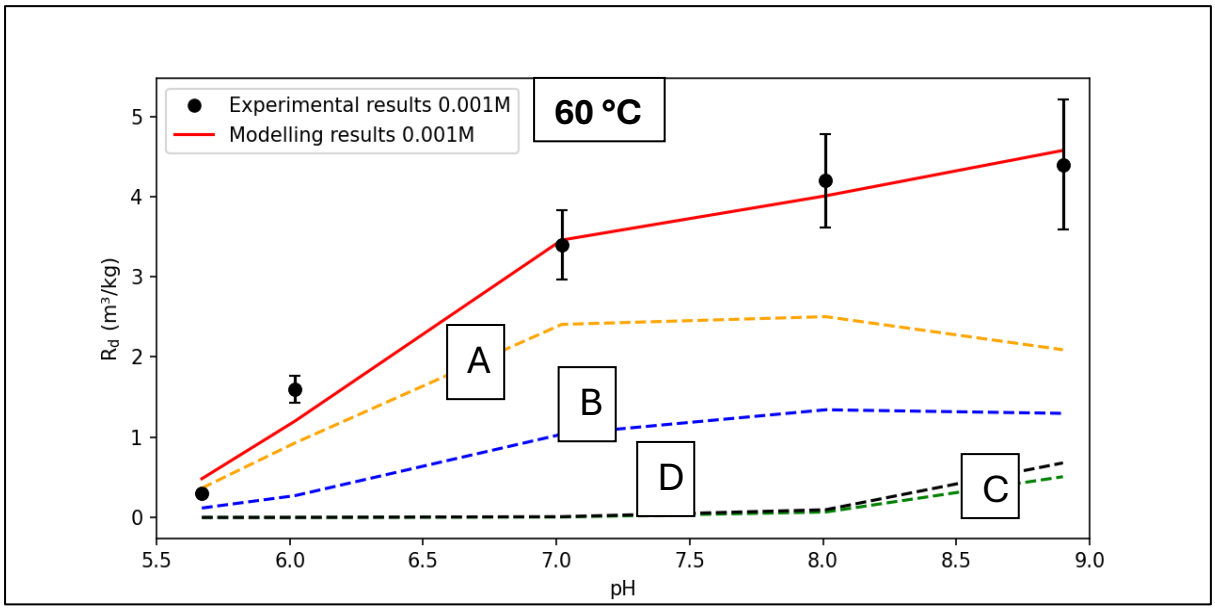

Figure 3-11: Results for barium sorption onto biotite mineral in 0.001 M $NaClO_4$ solution at 60 ºC (measurements (symbols) and modelling results (continuous lines)), where the contributions of different Ba(II) species to its sorption are represented by different curves: (A: yellow line) BaX_2; (B: blue line) ≡SOBa^+; (C: green line) ≡SOBaOH; (D: black line) XBaOH

The fact that the ion-exchange surface species BaX_2 is dominant except possibly at the very highest pH value may explain the lack of temperature dependency of barium sorption. This behavior of barium is in contrast to that of cesium, where the surface complex ≡SOCs was dominant over the ion-exchange species CsX and showed a marked positive temperature dependency. From these two cases, one may conclude that surface complexation may be a more temperature-dependent process than ion exchange. A summary of the surface reactions used in modelling is given in Table 6.

Table 6: Surface complexation and cation-exchange reactions and their associated constants (log k) for Ba(II) at 40 and 60 °C at zero ionic strength

Reaction		**Log k (40 °C)**	**Log k (60 °C)**
$\equiv SO^- + Ba^{2+} \leftrightarrow \equiv SOBa^+$		5.3 ± 0.3	5.9 ± 0.4
$\equiv SO^- + Ba(OH)^+ \leftrightarrow \equiv SOBaOH$		9.3 ± 0.3	9.7 ± 1.1
$\equiv SOH + Ba^{2+} \leftrightarrow \equiv SOHBa^{2+}$		Not significant*	Not significant*
$NaX + BaOH^+ \leftrightarrow BaOHX + Na^+$		6.1 ± 0.5	5.2 ± 0.3
Reaction/Ionic Strength at 40 °C	**Log k (0.001M)**	**Log k (0.01M)**	**Log k (0.1M)**
$Ba^{2+} + 2NaX \leftrightarrow BaX_2 + 2Na^+$	– 0.5	0.3	1.2
Reaction/Ionic Strength at 60 °C			
$Ba^{2+} + 2NaX \leftrightarrow BaX_2 + 2Na^+$	– 0.6	0.5	0.7

*The surface complex did not improve the fitting of the model to the sorption data.

The selectivity coefficients for cation exchange were allowed to vary across the series of ionic strengths, and the large standard deviations of the average results indicate that for barium the coefficients may not be treated as constants. The average log k values for ion exchange are –0.3±0.9 (40 °C) and 0.2±0.7 (60 °C).

In conclusion, the temperature had a small effect on barium sorption. In contrast to the case of cesium, the impact of temperature on barium sorption in 0.001 and 0.01 M $NaClO_4$ solutions was very low at all pH levels. On the other hand, at the highest ionic strength (0.1 M), an increase in barium sorption with temperature was seen at high pH levels (pH > 6), which may be attributable to the suppression of ion exchange by the effect of increased Na^+ concentration, which caused surface complexation to gain more influence. At pH < 6, the impact of temperature was negligible.

In contrast to cesium sorption, barium sorption shows a limited influence from increased temperature. However, similar to the case of cesium, an increased ionic strength and decreased pH suppress barium sorption by Na^+ and H^+ competition mechanisms, respectively. These are effective for both surface complexation (cesium) and ion exchange (barium).

3.5 Sorption modelling results of cobalt at 40 and 60 °C

The experimental and modeling results for Co sorption onto biotite for three ionic strengths and five pH values at 40 and 60 °C are shown in Figs. 3-12 and 3-13, respectively. The complete datasets can be found in Appendix A.

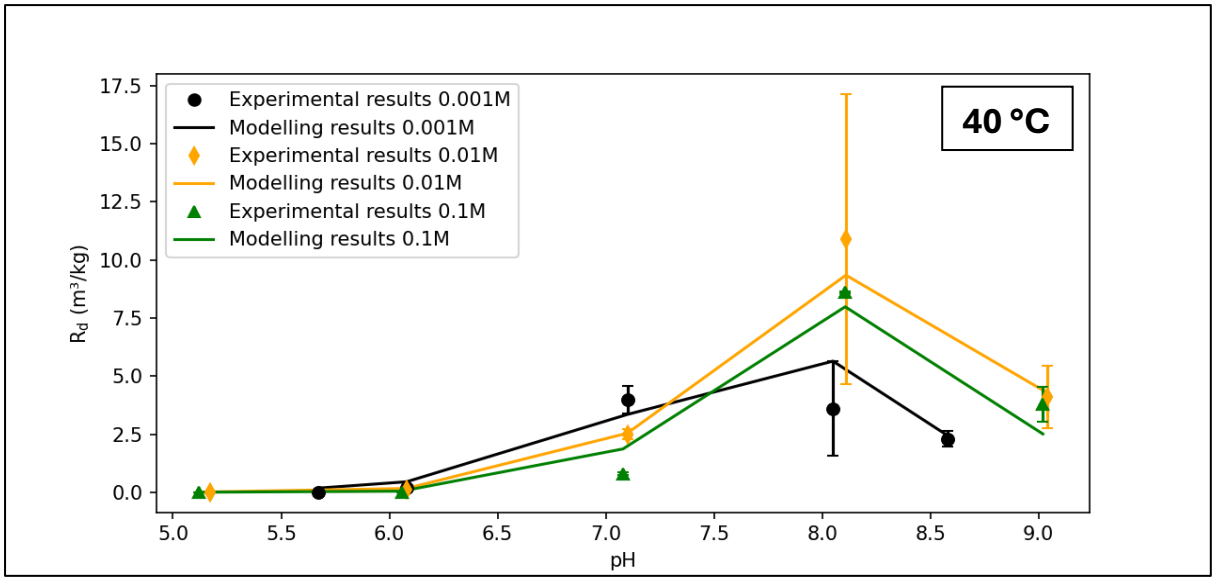

Figure 3-12: Cobalt sorption onto biotite mineral in 0.001, 0.01, and 0.1 M $NaClO_4$ solution as a function of pH at 40 °C: measurements (symbols) and modelling results (continuous lines)

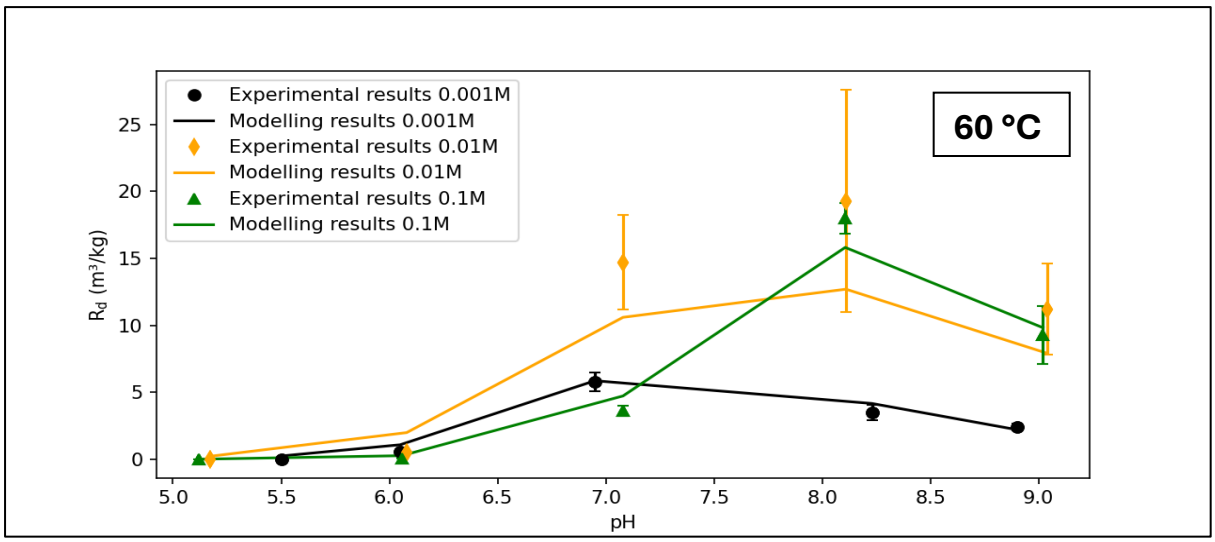

Figure 3-13: Cobalt sorption onto biotite mineral in 0.001, 0.01, and 0.1 M $NaClO_4$ solution as a function of pH at 60 °C: measurements (symbols) and modelling results (continuous lines)

At both temperatures, the R_d values of cobalt are considerably reduced at low pH values, a behavior that is very similar to those of both cesium and barium and that can be related to increased competition from H^+ for the sorption sites. The temperature has a relatively large positive effect on cobalt sorption. The results also suggest that the ionic strength has only a minor impact on cobalt uptake, especially in comparison with that of barium (Figs. 3-8 and 3-9). This finding could be an indication of the formation of strong cobalt surface complexes on the biotite surface.

Cobalt sorption increases from pH 6 to 8 and begins to decline from pH 8 to 9 for all three ionic strengths and at both 40 and 60 ºC. This type of distinct sorption "edge" is typical for surface complex formation due to the distinct pKa values for the deprotonation of sites. The modelling results indicate that no intermixing of ion exchange occurs. The sorption is then essentially governed by the pK_{a2} value of biotite, which is approximately 7, as determined from the titration data (Table 3). Similar results were reported following a study of the effects of ionic strength on cation sorption to oxide (Luetzenkirchen, 1997). The sharp increase in sorption from pH 6 to 8 signifies that surface complexation, rather than ion exchange, is responsible for cobalt sorption.

In order fit the cobalt sorption behavior onto biotite, three surface complexes ($\equiv SOCo^+$, $\equiv SOCoOH$, $\equiv SOCo(OH)_2^-$) and one ion-exchange species (CoX_2) were considered. However, because the cobalt sorption at pH < 6 is very low, any contribution of ion exchange to cobalt sorption is negligible and the weak surface complex $\equiv SOHCo^{2+}$ is not formed.

Figs. 3-14 (40 °C) and 3-15 (60 °C) display the modeling results for 0.001 M $NaClO_4$, and thoes for 0.01 and 0.1 M are shown in Appendix B.

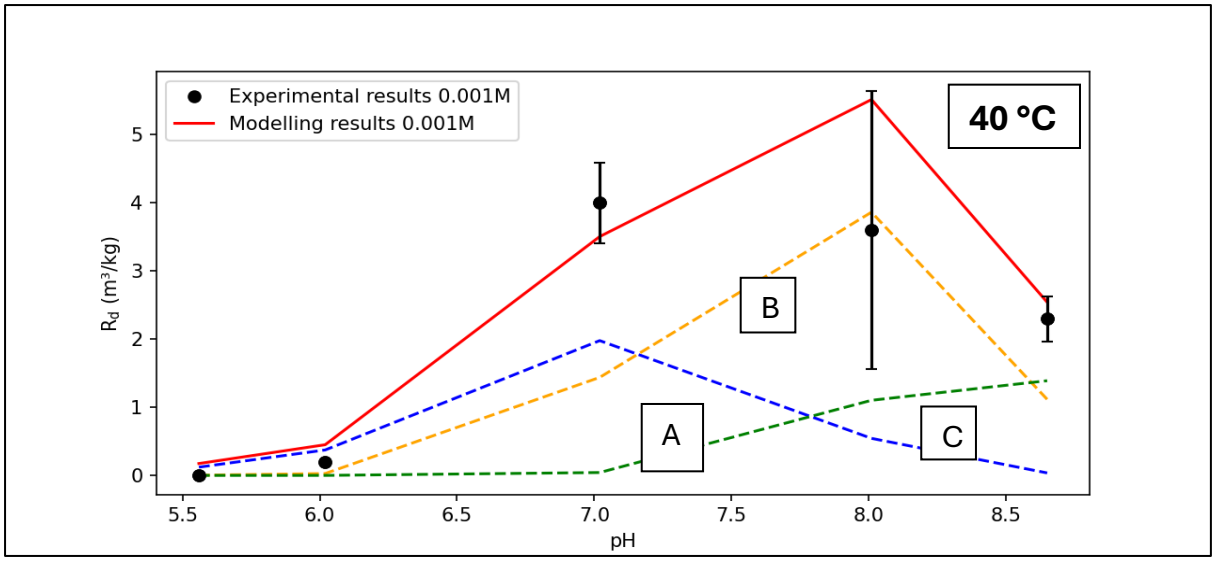

Figure 3-14: Results for cobalt sorption onto biotite mineral in 0.001 M $NaClO_4$ solution at 40 ºC (measurements (symbols) and modelling results (continuous lines)), where the contributions of different Co(II) species to cobalt sorption are represented by different curves: (A: blue line) ≡$SOCo^+$; (B: yellow line) ≡SOCoOH; (C: green line) ≡ $SOCo(OH)_2^-$

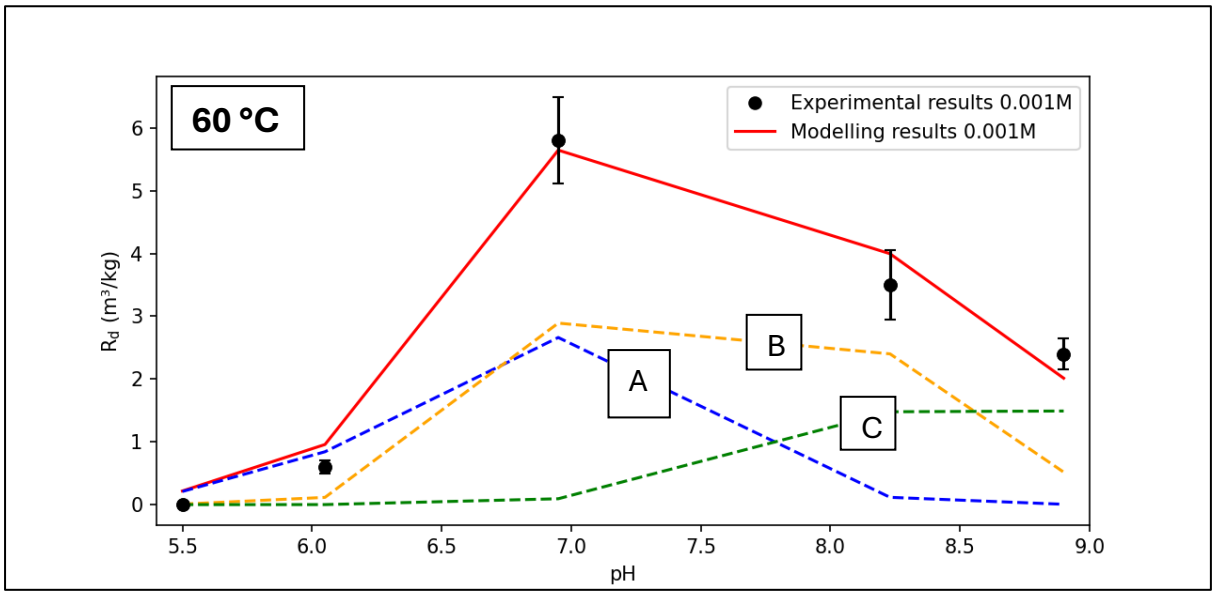

Figure 3-15: Results for cobalt sorption onto biotite mineral in 0.001 M $NaClO_4$ solution at 60 ºC (measurements (symbols) and modelling results (continuous lines)), where the contributions of different Co(II) species to cobalt sorption are represented by different curves: (A: blue line) ≡$SOCo^+$; (B: yellow line) ≡SOCoOH; (C: green line) ≡ $SOCo(OH)_2^-$.

The cobalt sorption modeling results show a predominant surface complexation mechanism, which should be in line with the reasoning above regarding a correlation between surface complexation and a strong influence from temperature changes, as confirmed by comparing the two datasets. Cobalt shows a strongest effect from temperature (Figs. 3-12 and 3-13) with the maximum R_d value (at approximatly pH 8) increasing from 8 to 19.3 m^3/kg for 0.1M $NaClO_4$.

The surface complexation reactions that were used are listed in Table 7, along with their optimized constants.

Table 7: Modelled surface complexation reactions and their associated constants (log k) for Co (II) at 40 and 60 °C at zero ionic strength

Reaction	**Log k (40 °C)**	**Log k (60 °C)**
$\equiv SO^- + \mathrm{Co}^{2+} \leftrightarrow \equiv \mathrm{SOCo}^+$	5.6 ± 0.4	6.4 ± 0.4
$\equiv SO^- + \mathrm{Co(OH)}^+ \leftrightarrow \equiv \mathrm{SOCoOH}$	8.0 ± 0.7	8.3 ± 1.0
$\equiv SO^- + Co(OH)_2 \leftrightarrow \equiv \mathrm{SOCo(OH)}_2^-$	5.7 ± 0.6	6.7 ± 1.3
$\equiv \mathrm{SOH} + \mathrm{Co}^{2+} \leftrightarrow \equiv SOHCo^{2+}$	Not significant*	Not significant*
$\mathrm{Co}^{2+} + 2\mathrm{NaX} \leftrightarrow \mathrm{CoX}_2 + 2\mathrm{Na}^+$	Not significant*	Not significant*

*The surface complex did not improve the fitting of the model to sorption data.

All the reaction constants for the cobalt surface complexes increase with temperature. In conclusion, cobalt sorption increased with temperature at all three ionic strengths investigated. This effect was ascribed to the formation of the surface complexes ($\equiv\mathrm{SOCo}^+$, $\equiv \mathrm{SOCoOH}$, and $\equiv \mathrm{SOCo(OH)}_2^-$). The sorption of cobalt was unique among those of the tracers investigated in this study in that sorption was modelled as surface complexation without any involvement of ion exchange. The observed decrease in sorption for cobalt above pH 8 can therefore likely be assigned primarily to the formation of aqueous hydroxide complexes. At low pH, cobalt sorption decreased rapidly, most likely due to the protonation of the surface complexation sites.

3.6 Sorption modelling results of europium at 40 and 60 °C

The modeling and experimental data for all ionic strengths *(0.001, 0.01, and 0.1 M)* at 40 and 60 ºC are shown in an examples Fig. 3-16 and 3-17. The complete dataset is shown in Appendix A.

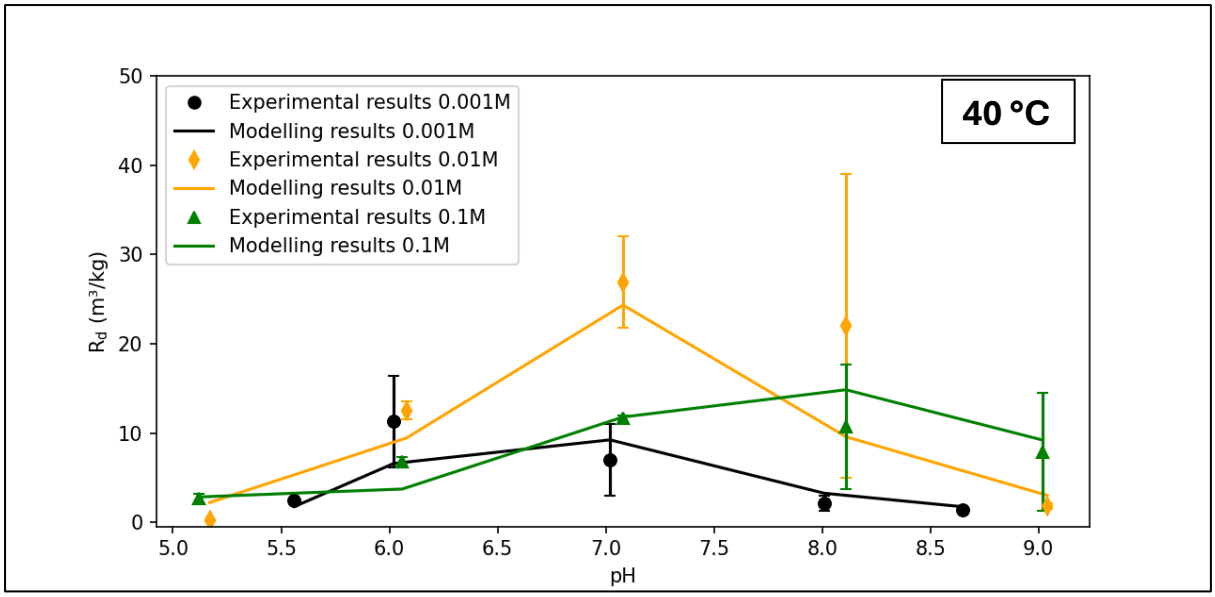

Figure 3-16: Europium sorption onto biotite mineral in 0.001, 0.01, and 0.1 M $NaClO_4$ solution as a function of pH at 40 °C: measurements (symbols) and modelling results (continuous lines)

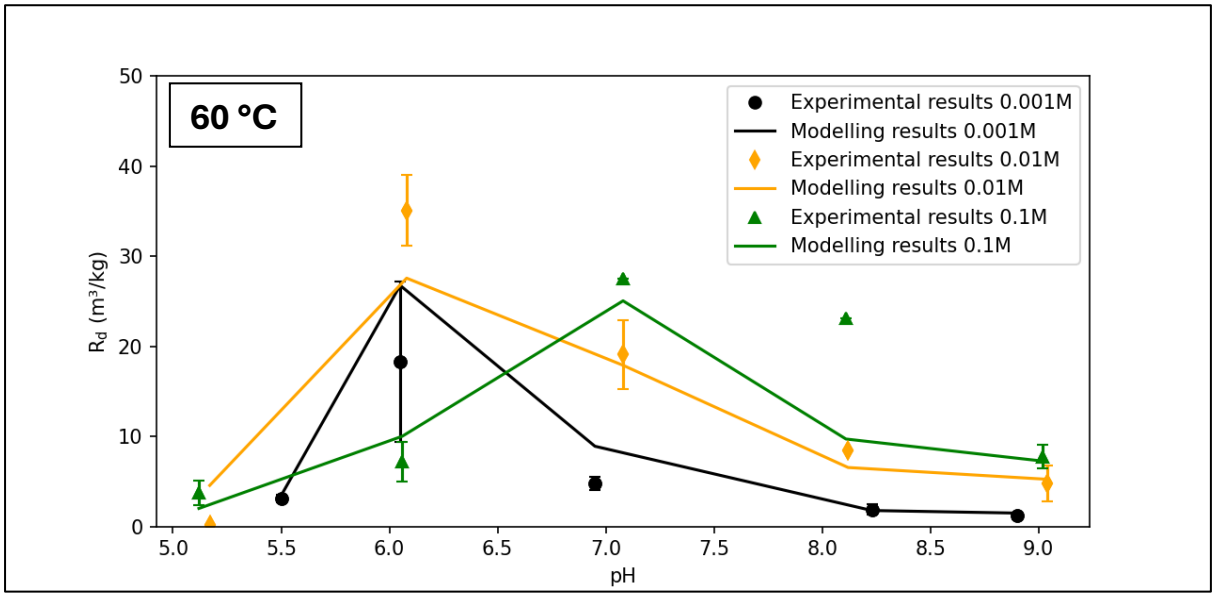

Figure 3-17: Europium sorption onto biotite mineral in 0.001, 0.01, and 0.1 M $NaClO_4$ solution as a function of pH at 60 °C: measurements (symbols) and modelling results (continuous lines)

Europium sorption increases as the pH increases to approximately pH 6–7 at both temperatures and then gradually decreases as the pH increase further to 9. The decrease in the distribution coefficient can probably be attributed to aqueous hydroxyl complex formation. The influence of ionic strength is not particularly pronounced. At the peak sorption point, the temperature has a comparatively large positive effect on europium sorption, increasing R_d from approximately 11.3 to 35.1 m^3/kg for 0.01M $NaClO_4$.

Comparing the europium sorption results with the results for the other three elements indicates that europium may mainly sorb by surface complexation due to the significant temperature effect and limited ionic strength effect.

Europium sorption onto biotite was modelled by considering four surface species: $\equiv SOEu^{2+}$,$\equiv SOEu(OH)^{+}$, $\equiv SOEu(OH)_2$, and EuX_3 for all three $NaClO_4$ solutions (0.001, 0.01, and 0.1 M) at both temperatures. The other species considered was a weak surface complex ($\equiv SOHEu^{+}$), but it had a negligible contribution to the model fitting and thus was excluded from the modeling.

The data fitting results for the case of 0.001 M $NaClO_4$ at 40 and 60 ºC are shown in Figs. 3-18 and 3-19, respectively. The results for 0.01 and 0.1 M $NaClO_4$ can be found in Appendix B.

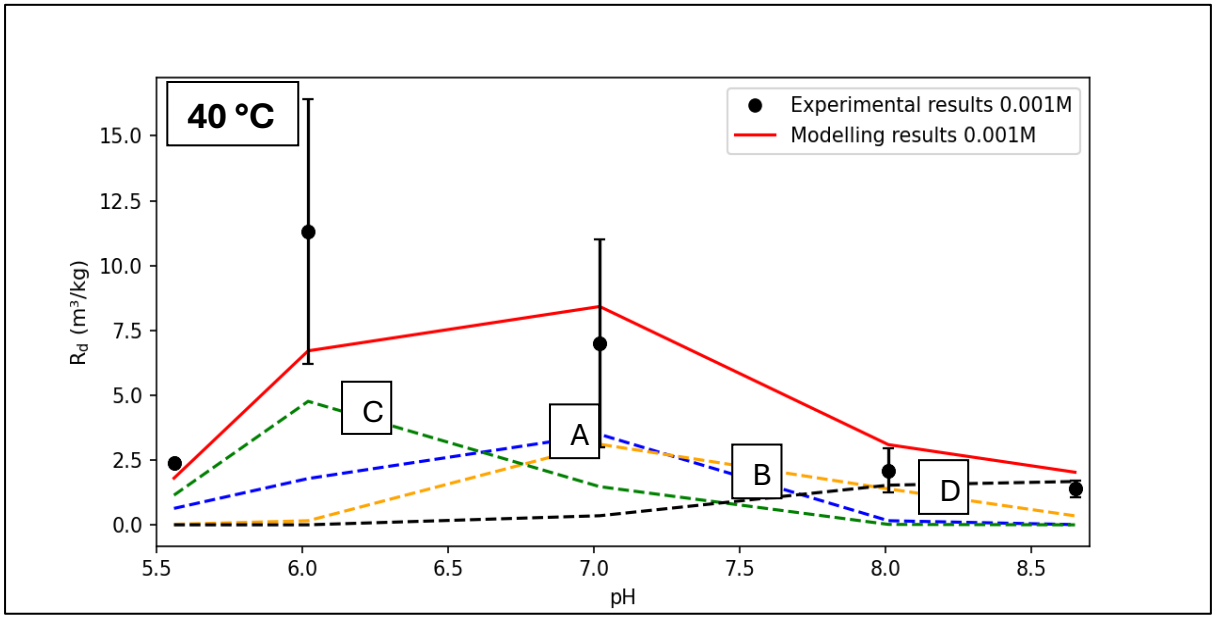

Figure 3-18: Results for europium sorption onto biotite mineral in 0.001 M $NaClO_4$ solution at 40 ºC (measurements (symbols) and modelling results (continuous lines)), where the contributions of different Eu(III) species to its sorption are represented by different curves: (A: blue line) $\equiv SOEu^{2+}$; (B: yellow line) $\equiv SOEu(OH)^{+}$; (C: green line) EuX_3; (D: black line) $\equiv SOEu(OH)_2$

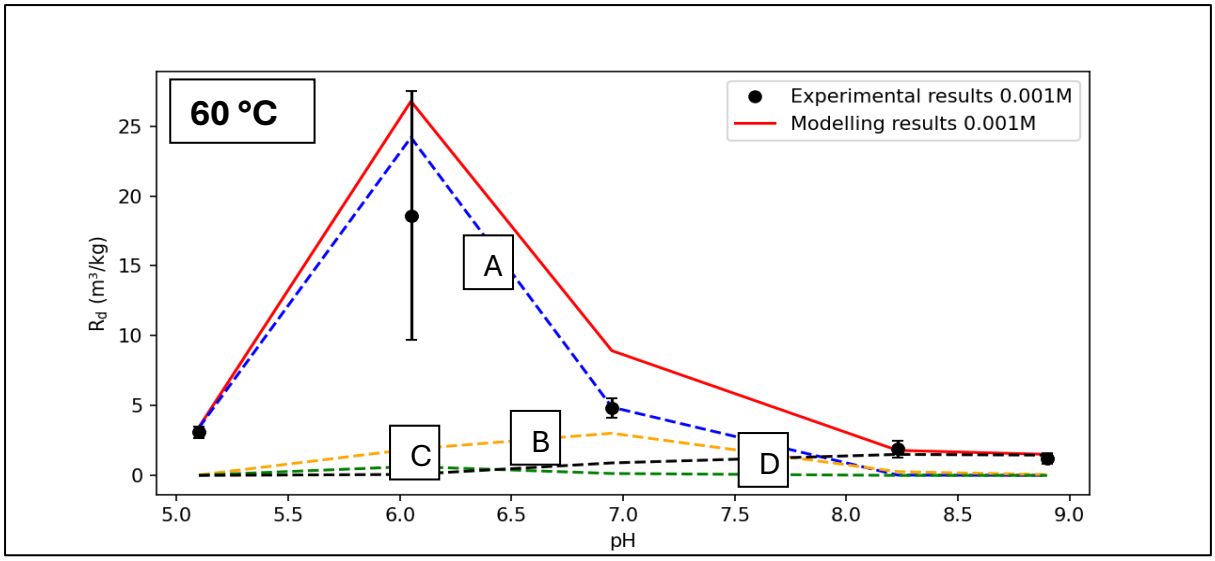

Figure 3-19: Results for europium sorption onto biotite mineral in 0.001 M $NaClO_4$ solution at 60 ºC (measurements (symbols) and modelling results (continuous lines)), where the contributions of different Eu(III) species to its sorption are represented by different curves: (A: blue line) ≡ $SOEu^{2+}$; (B: yellow line) ≡ $SOEu(OH)^{+}$; (C: green line) EuX_3; (D: black line) ≡ $SOEu(OH)_2$

The data for 40 °C indicate that at a pH of approximately 5, the sorption is dominated by the ion-exchange species EuX_3. However, when the pH increases, the europium uptake is chiefly governed by surface complexation species ≡ $SOEu^{2+}$ and ≡ $SOEu(OH)^{+}$. This phenomenon is probably related to the pK_{a2} value of approximately 7 for biotite.

At 60 ºC (Fig. 3-19), the modelling results suggest that for all three ionic strengths, at a pH of approximately 6, the europium uptake is predominantly due to the ≡ $SOEu^{2+}$ species. Apparently, this surface complex is enhanced over the other surface species by the increased temperature.

The surface complexation reactions that were used are listed in Table 8, along with their optimized constants.

Table 8: Surface complexation and cation-exchange reactions and their associated constants (log k) for Eu (III)

Reaction	**Log k (40 °C)**	**Log k (60 °C)**
$\equiv \boldsymbol{SO^- + Eu^{3+} \leftrightarrow \equiv SOEu^{2+}}$	6.5 ± 0.8	8.1 ± 0.2
$\equiv \boldsymbol{SO^- + Eu(OH)^{2+} \leftrightarrow \equiv SOEu(OH)^{+}}$	6.9 ± 1.3	8.1 ± 1.2
$\equiv \boldsymbol{SO^- + Eu(OH)_2^{+} \leftrightarrow \equiv SOEu(OH)_2}$	5.6 ± 1.2	6.6 ± 1.2

Reaction/Ionic Strength at 40 °C	0.001 M	0.01 M	0.1 M
$\boldsymbol{Eu^{3+} + 3NaX \leftrightarrow EuX3 + 3Na^{+}}$	log k = –2.7	log k = 0.3	log k = 3.3
Reaction/Ionic Strength at 60 °C	0.001 M	0.01 M	0.1 M
$\boldsymbol{Eu^{3+} + 3NaX \leftrightarrow EuX3 + 3Na^{+}}$	log k = –2.9	log k = –0.2	log k = 3.1

The selectivity coefficient for EuX_3 species was allowed to vary with ionic strength, as shown in Table 8. The relatively large variation indicates that this parameter is not constant. Instead, the temperature has a consistent negative effect on this parameter.

3.7 Thermodynamic parameters

The most common and conventional method of quantifying the effect of temperature on radionuclide sorption is to derive the thermodynamic parameters for the sorption reactions, such as enthalpy and entropy. Using the van't Hoff formalism, this information can be deduced by plotting the temperature dependence of the reaction constant ((log K) vs. 1/T) by using Eq. 14:

$$Log\ K = \frac{\Delta S^o}{R} - \frac{\Delta H^o}{RT} \qquad \text{(Eq. 14)}$$

where ΔH^o and ΔS^o are the enthalpy and entropy of the surface complexation or ion-exchange reaction, respectively; R is the gas constant; and T is the absolute temperature.

The reaction constants (log K) for cesium, barium, cobalt, and europium were optimized using PHREEQC and PYTHON. The plot of log K vs. 1/T was a straight line with a gradient of $-\Delta H^o/R$ and an intercept of $\Delta S^o/R$. Thus, the enthalpy and entropy of the reactions were constant in the investigated temperature range, as illustrated in Fig. 3-20. The dataset shown in the Fig. 3-20 is extended with the constants determined at 25 °C in our previous work (Kumar

et al., submitted manuscript). Table 9 shows ΔH^o and ΔS^o for the sorption reactions of all elements based on the ion-exchange and surface complexation constants, as discussed above.

Table 9: Thermodynamic parameters for the sorption of cesium, barium, cobalt, and europium onto biotite

Surface complex/ion-exchange species for elements	ΔH^0 (**kJ mol^{-1}**)	ΔS^0(**JK^{-1}mol^{-1}**)
Cesium		
≡SOCs	38.1±0.9	165.1±0.9
CsX	–18.6±0.9	– 47.9±0.9
Barium		
≡ SOBa^{+}	20.9±0.9	111.6±0.9
≡ SOBaOH	12.4±0.9	117.6±0.9
BaX_2	–6.3±0.9	16.71±0.9
XBaOH	–46.1±0.9	–95.4±0.9
Cobalt		
≡ SOCo^{+}	22.6±0.9	119.9 ±0.9
≡ SOCoOH	23.5±0.9	140.4 ±0.9
≡ $SOCo(OH)_2^-$	45.3±1.0	191.8±1.0
Europium		
≡ SOEu^{2+}	8.3±0.9	76.4±0.9
≡ SOEuOH^{+}	43.0 ±0.8	195.6±0.8
≡ $SOEu(OH)_2$	32.2±0.9	150.9±0.9
EuX_3	–9.6±0.9	–28.7 ±0.9

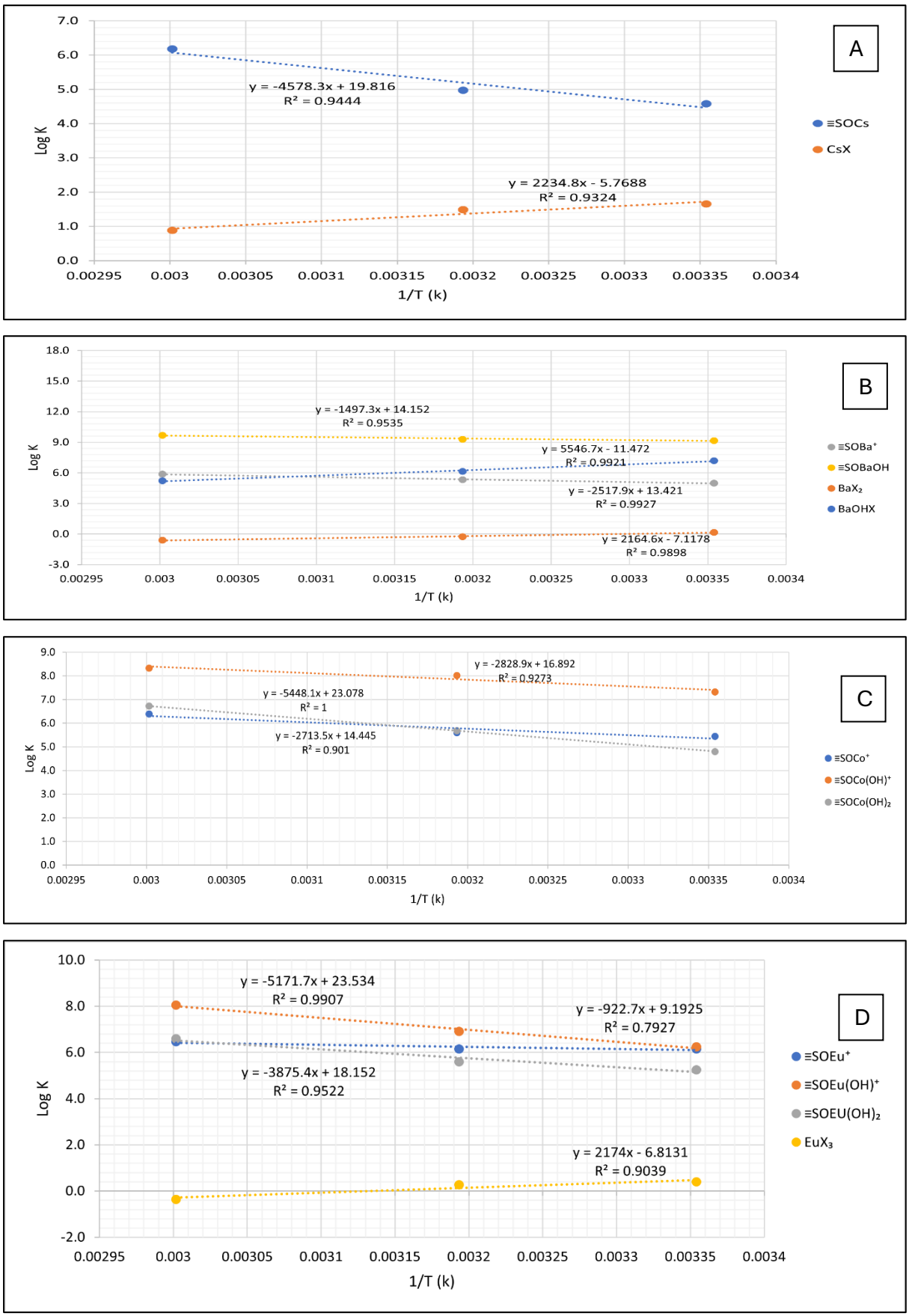

Figure 5-29: Van't Hoff plots were used to derive ion-exchange and surface complexation constants for ^{134}Cs (A), ^{133}Ba (B), ^{60}Co (C) and ^{152}Eu (D). The enthalpy of the sorption reactions was determined using the slopes of the correlations.

The thermodynamic parameter results show that both the enthalpy and entropy for the cesium, barium, cobalt, and europium surface complexes are positive. The Gibbs free energy is negative (ln K >1), implying that the surface complexes are entropy-driven, which can be attributed to the formation of the inner sphere complex, where the hydration shell of the adsorbing species is at least partially released.

The sorption enthalpy for ≡SOCs was 38.1±0.9 kJ/mol. The barium sorption enthalpy values were 20.9±0.9 and 12.4±0.9 kJ/mol for ≡ $SOBa^+$ and ≡ SOBaOH, respectively. The enthalpy for the ≡$SOCo^+$, ≡SOCoOH, and ≡ $SOCo(OH)_2^-$ complexes of cobalt was 22.4±0.9, 23.5±0.9, and 45.3±1.0 kJ/mol, respectively. For europium, the enthalpy was determined to be 8.3±0.9, 43.0 ±0.8, and 32.2±0.9 kJ/mol for the ≡ $SOEu^{2+}$, ≡ $SOEuOH^+$, and ≡ $SOEu(OH)_2$ complexes, respectively.

In general, cations are very well solvated in water. In order to sorb these ions on mineral surfaces, the dehydration of water molecules from the cation is required. The enthalpy values calculated from the temperature-dependent equilibrium constants (Table 9) for the sorption reaction are endothermic (heat-adsorbing), which means that a significant quantity of energy is necessary for the partial desolvation of water molecules from cations during the formation of the inner sphere complex. During this process, water molecules are released from the hydration sphere, resulting in positive entropy.

On the other hand, the enthalpy values for the exchange surface species CsX, BaX_2, XBaOH, and EuX_3 species were determined to be –18.6±0.9, –6.3±0.9, –46.1±0.9, and –9.6±0.9 $K\text{Jmol}^{-1}$, respectively and consequently exothermic (heat-releasing). The negative enthalpy values for CsX, BaX_2, XBaOH, and EuX_3, which are in contrast with the positive enthalpy values for the other surface complexes, as outlined above, could be explained by the hypothesis that these species are indeed of the ion-exchange type, which need minimal cation dehydration before sorbing on the cation-exchange site (NaX) of biotite and hence have a little effect on entropy. Instead the exchange is driven by the exothermic replacement of Cs^+, Ba^{2+}, and Eu^{3+} in solution by Na^+ , which is a much better solvated cation than the other three cations. That ion-exchange is mainly a solvation-promoted process rather than an adsorption-promoted process have been demonstrated with combined microcalorimetry and modeling studies (Rotenberg, et al., 2009).

4. Conclusion

A batch sorption experiment was conducted to investigate the sorption of ^{134}Cs, ^{133}Ba, ^{60}Co, and ^{152}Eu in a mixture at tracer concentration (on the order of 10^{-8} M), on sodium-converted biotite. The experiment was conducted in triplicate at pH 5–9 with background electrolytic solutions containing 0.001, 0.01, and 0.1 M $NaClO_4$ at 40 and 60 °C. All tracers were considerably affected by the pH, but the ionic strength levels affected mainly cesium and barium.

The temperature-dependence study showed that the sorption of cesium, cobalt, and europium was influenced by temperature; however, barium sorption showed little dependence on temperature.

The modelling suggests that this behavior can be explained by formation of both surface complexes and ion-exchange species. The temperature dependences of the modelled reaction constants and coefficients can be used to verify the type of binding to the surface. This ability represents an advantage of this approach over spectroscopic methods that are used to identify sorption mechanisms because the latter usually operate at much higher sorbing element concentrations. The temperature variation method, on the other hand, works under exactly the same conditions as those under which the binding constants are determined.

For the ion-exchange species, a very low negative enthalpy was calculated for Cs^+, Ba^{2+}, and Eu^{3+}, which shows that these species may undergo sorption on the biotite surface via an ion-exchange process. The surface complexes, on the other hand, had positive enthalpy, which implies that the surface complexation reactions are endothermic and entropically driven. The positive enthalpy of the complexes may indicate that they undergo sorption onto the mineral surface, forming an inner-sphere complex.

Acknowledgment

This research was supported by grants from SSM (Swedish Radiation Safety Authority). We thank Dr. A.M. Jakobsson for her valuable comments, which helped us improve the manuscript.

References

Allard, B. & Beall, G. a. K. T., 1980. The sorption of actinides in igneous rocks. *Nuclear Technology,* pp. 474-480.

Andersson, M. et al., 2008. *Development of methodology for evaluation of long-term safety aspects of organic cement paste components,* Olkiluoto: POSIVA.

Andersson, M. et al., 2008. *Development of methodology for evaluation of long-term safety aspects of organic cement paste components Working Report 2008-28,* Olkiluoto, Finland: Posiva Oy.

Berubé, Y. G., Onoda, G. Y. & De Bruyn, P. L., 1967. Proton adsorption at the ferric oxide/aqueous solution interface. *Surface Science,* Volume 8, pp. 448-461.

Bradbury, M. & Baeyens, B., 2002. Sorption of Eu on Na-and Ca-montmorillonites: Experimental investigations and modelling with cation exchange and surface complexation. *Geochim. Cosmochim. Acta,* Volume 66, pp. 2325-2334.

Bradbury, M. & Baeyens, B., 2009. Sorption modelling on illite Part I: Titration measurements and the sorption of Ni, Co, Eu and Sn. *Geochim. Cosmochim. Acta,* Volume 73, pp. 990-1003.

Bradbury, M. H. & Baeyens, B., 2000. A generalized sorption model for the concentration dependent uptake of caesium by argillaceous rocks. *Journal of Contaminant Hydrology,* Volume 42, pp. 141-163.

Bray, A. W., Benning, L. G., Bonneville, S. & Oelkers, E. H., 2014. Biotite surface chemistry as a function of aqueous fluid composition. *Geochi. Cosmochim. Acta,* Volume 128, pp. 58-70.

Bray, A. W. et al., 2015. Effect of pH, grain size, and organic ligands on biotite weathering rates. *Geochim. Cosmochim. Acta,* Volume 164, pp. 127-145.

Bray, A. W. et al., 2015. The effect of pH, grain size and organic ligands on biotite weathering rates. *Geochimica et Cosmochimica Acta,* Volume 164, pp. 127-145.

Brunauer, S., Emmet, P. H. & Teller, E., 1938. Adsorption of gases in multimolecular layers. *J. Am. Chem. Soc.*, Volume 60, pp. 309-319.

Brunauer, S., Emmet, P. H. & Teller, E., 1938. Adsorption of gases in multimolecular layers. *Journal of the American Chemical society*, Volume 60, pp. 309-319.

Brunauer, S., Emmet, P. H. & Teller, E., 1938. Adsorption of gases in multimolecular layers. *J. Am. Chem. Soc.*, Volume 60, pp. 309-319.

Charlton, S. R. & Parkhurst, D. L., 2011. Modules based on the geochemical model PHREEQC for use in scripting and programming languages. *Comput. Geosci.,* Volume 37, pp. 1653-1663.

Cornell, R. M., 1993. Adsorption of cesium on minerals: A review. *J Radioanal. Nucl. Chem.,* Volume 171, pp. 483-500.

Crank, J., 1979. *The Mathematics of diffusion.* 2nd ed. New York: Oxford University Press.

Crawford, J., 2010. *Bedrock Kd data and uncertainty assessment for application in SR-Site geosphere transport calculations (R-10-48),* Stockholm: Svensk Kärnbränslehantering ABB.

Crawford, J., 2010. *Bedrock Kd data and uncertainty assessment for application in SR-Site geosphere transport calculations (R-10-48),* Stockholm: Svensk Kärnbränslehantering AB.

Davis, J. A., Coston, J. A., Kent, D. B. & Fuller, C. C., 1998. Application of the surface complexation concept to complex mineral assemblages. *Env. Sci. Technol.,* Volume 32, pp. 2820-2828.

Davis, J. A., Meece, D. E., Kohler, M. & Curtis, G. P., 2004. Approaches to surface complexation modeling of uranium(VI) adsorption on aquifier sediments. *Geochim. Cosmochim. Acta,* Volume 68, pp. 3261-3641.

Drake, H., Sandström, B. & Tullborg, E.-L., 2006. *Mineralogy and geochemistry of rocks and fracture fillings from Forsmark and Oskarshamn: Compilation of data for SR-Can (R-06-109),* Stockholm: Svensk Kärnbränslehantering AB.

Dubois, I., 2011. *Specific surface area of some minerals commonly found in granite*. Stockholm: Kungliga Tekniska Högskolan.

Ekberg, C. & Brown, P. L., 2016. *Hydrolysis of metal ions. Vol. 1 and 2.*. s.l.:Wiley-VCH.

Eveliina, M. et al., 2016. Behavior of Cs in Grimsel granodiorite: sorption on main minerals and crushed rock. *Radiochim. Acta,* Volume 104, pp. 575-582.

Fabritius, O. et al., 2022. Radium sorption on biotite; surface complexation modeling study. *Applied Geochemistry,* Volume 140, p. 105289.

Fukushi, K. et al., 2013. Sorption of Eu(III) on granite: EPMA, LA-ICP-MS, batch and modeling studies. *Environ. Sci. Technol.,* Volume 47, pp. 12811-12818.

Furuya, K. et al., 1997. *Sorption of plutonium on a biotite mineral,* Tohoku: Science Reports of the Research Institutes Tohoku University, Series A Physics.

Gran, G., 1950. Determination of the equivalent point in potentiometric titrations. *Acta Chem. Scand.,* Volume 4, pp. 557-559.

Hakanen, M., Ervanne, H. & Puukko, E., 2012. *Safety case for the disposal of spent nuclear fuel at Olkiluoto - Radionuclide migration parameters for the geosphere (2012-41),* Olkiluoto, Finland: Posiva Oy.

Hedin, A. & Olsson, O., 2016. Crystalline rock as a repository for Swedish spent nuclear fuel. *Elements,* pp. 247-252.

Holgersson, S., 2012. Studies on batch sorption methodologies: Eu sorption onto Kivetty granite. *Procedia Chemistry,* Volume 7, pp. 629-640.

Holgersson, S., Drake, H., Karlsson, A. & Krall, L., 2024. Biotite dissolution kinetics at pH 4 and 6.5 under anaerobic conditions and the release of dissolved Fe(II). *Chemical Geology,* Volume 662, p. 122204.

Holgersson, S., Drake, H., Karlsson, A. & Krall, L., 2024. Biotite dissolution kinetics at pH 4 and 6.5 under anaerobic conditions and the release of dissolved Fe(II). *Chem.Geol.,* Volume 662, p. 122204.

Holgersson, S. & Kumar, P., 2023. A literature review on thermodynamic sorption models of radionuclides with some selected granitic minerals. *Front. Nucl. Eng.,* Volume 2, p. 1227170.

Holgersson, S. & Kumar, P., 2023. A literature review on thermodynamic sorption models of radionuclides with some selected granitic minerals. *Front. Nucl. Eng.,* p. 1227170.

Hunter, R. .., 1989.

Jakobsson, A.-M., 1999. *Measurement and modelling using surface complexation of cation (II to VI) sorption onto mineral oxides*. Göteborg: Chalmers University of Technology, Department of Nuclear Chemistry.

Jakobsson, A., Albinsson, Y. & Rundberg, R., 1998. *Studies of surface complexation of H+ , NpO2+, Co2+, Th4+ onto TiO2 and H+, UO22+ onto alumina (TR-98-15),* Stockholm: Svensk Kärnbränslehantering AB.

Jordan, N. et al., 2024. A critical review of the solution chemistry, solubility, and thermodynamics of europium: Recent advances on the Eu(III) hydrolysis. *Coordin. Chem. Rev.,* Volume 510, p. 215702.

Kosmulski, M., 2020. The pH dependent surface charging and points of zero charge. VIII Update.. *Adv.Colloid Interface Sc.,* p. 102064.

Kumar, P., Holgersson, S. & Ekberg, C., in press. Sorption of Cs, Ba, Co and Eu onto biotite at 40 and 60 C - a combined experimental and modelling study. *J. Contamin. Hydrol.*.

Kyllönen, J. et al., 2014. Modeling of cesium sorption on biotite using cation exchange selectivity coefficients. *Radiochimica Acta,* Volume 102, pp. 919-929.

Kyllönen, J. et al., 2014. Modeling of cesium sorption on biotite using cation exchange selectivity coefficients. *Radiochim. Acta,* Volume 102, pp. 919-929.

Kyllönen, J. et al., 2014. Modeling of cesium sorption on biotite using cation exchange selectivity coefficients. *Radiochim. Acta,* Volume 102, pp. 919-929.

Li, X. et al., 2018. Sorption of Se species on mineral surfaces, part I: batch sorption and multi-site modelling. *Applied Geochemistry,* Volume 95, pp. 147-157.

Li, X. et al., 2020. Multi-site surface complexation modelling of Se (IV) sorption on biotite. *Chemical Geology,* Volume 533, p. 119433.

Li, X. et al., 2020. Multi-site surface complexation modelling of Se(IV) sorption on biotite. *Chem. Geol.,* Volume 533.

Luetzenkirchen, J., 1997. Ionic strength effects on cation sorption to oxides: Macroscopic observations and their significance in microscopic interpretation. *J Colloid. Interface Sci.,* Volume 195, pp. 149-155.

Luetzenkirchen, J., 1997. Ionic strength effects on cation sorption to oxides: Macroscopic observations and their significance in microscopic interpretation. *J. Colloid. Interface Sci.,* Volume 195, pp. 149-155.

Macht, F., Eusterhues, K., Pronk, G. J. & Totsche, K. U., 2011. Specific surface area of clay minerals: Comparison between atomic force microscopy meaurements and bulk.gas (N2) and -liquid (EGME) adsorption methods. *App. Clay. Sci.,* pp. 20-26.

McKinley, J. P. et al., 2004. Microscale distribution of cesium sorbed to Bbiotite and muscovite. *Environ. Sci. Technol.,* Volume 38, pp. 1017-1023.

Miller , B. & Marcos, N., 2007. *Process report - FEPs and scenarios for a spent fuel repository at Olkiluoto (Posiva Report 2007-12),* Olkiluoto, Finland: Posiva Oy.

Muuri, E. et al., 2018. The sorption and diffusion of 133Ba in crushed and intact granitic rocks from the Olkiluoto and Grimsel in-situ test sites. *Applied Geochemistry,* Volume 89, pp. 138-149.

Muuri, E. et al., 2016. Bahavior of Cs in Grimsel granodiorite: sorption on main minerals and crushed rock. *Radiochemica Acta,* Volume 104, pp. 575-582.

Muuri, E. et al., 2016. Bahavior of Cs in Grimsel granodiorite: sorption on main minerals and crushed rock. *Radiochim. Acta,* Volume 104, pp. 575-582.

Muuri, E. et al., 2017. Cesium sorption and diffusion on crystalline rock: Olkiluoto casestudy. *Journal of Radioanalytical and Nuclear Chemistry,* Volume 311, pp. 439-446.

Nagy, K. L., 1995. Dissolution and precipitation kinetics of sheet silicates. *Rev. Mineral.,* Volume 31, pp. 173-225.

Nesse, W. D., 2000. *Introduction to mineralogy.* New York: Oxford University Press.

Parkhurst, D. L. & Appelo, C. A. J., 2021. *PHREEQC version 3: Computer Program for Speciation, Batch-Reaction, One-Dimensional Transport, and Inverse Geochemical Calculations.* s.l.:U.S. Geological Survey.

Payne, T. E. et al., 2013. Guidelines for thermodynamic sorption modelling in the context of radioactive waste disposal. *Environ. Modell. Softw.,* Volume 42, pp. 143-156.

Payne, T. E. et al., 2013. Guidelines for thermodynamic sorption modelling in the context of radioactive waste disposal. *Environ. Modell. Softw.,* Volume 42, pp. 143-156.

Puukko, E. et al., 2007. *Sorption of nickel and europium on biotite,* Moor Row, UK: Nuclear Decommisioning Authority.

Puukko, E. et al., 2007. Sorption of nickel and europium on biotite. *In FUNMIG 3rd Annual Meeting,* pp. 265-272.

Rodriguez-Cruz, S. & Jockusch, R. a. W. E., 1999. Hydration energies and structures of alkaline earth metal ions, M2+ (H2O) n, n= 5− 7, M= Mg, Ca, Sr, and Ba. *Journal of the American Chemical Society,* Volume 121, pp. 8898-8906.

Rotenberg, B. et al., 2009. On the driving force of cation exchange in clays: Insights from combined microcalorimetry experiments and molecular simulation. *Geochim. Cosmochim. Acta,* Volume 73, pp. 4034-4044.

Rovira, M. et al., 2008. Sorption of selenium (IV) and selenium (VI) onto natural iron oxides: goethite and hematite. *J. Hazard. Mater.,* Volume 150, pp. 279-284.

Schollenberger, C. & Simon, R., 1945. Determination of exchange capacity and exchangeable bases in soil—ammonium acetate method. *Soil Sci.,* Volume 59, pp. 13-24.

Selnert, E., Byegård, J. & Widestrand, H., 2008. *Forsmark site investigation - Laboratory measurements within the site investigation programme for the transprt properties of the rock, Final report (P-07-139),* Stockholm: Svensk Kärnbränslehantering AB.

SKB, 2010. *Design and production of the KBS-3 repository (TR-10-12),* Stockholm: Svensk Kärnbränslehantering AB.

SKB, 2011. *Long-term safety for the final repository for spent nuclear fuel at Forsmark Main report of the SR-Site project Volume III (TR-11-01),* Stockholm: Svensk Kärnbränslehantering AB.

SKB, 2011. *Long-term safety for the final repository for spent nuclear fuel at Forsmark, Main report of the SR-Site project. Vol I-III (TR-11-01),* Stockholm: Svensk Kärnbränslehantering AB.

SKBF/KBS, 1983. *Kärnbränslecykelns slutsteg,* Stockholm: Svensk Kärnbränsleförsörjning AB (Swedish Nuclear Fuel and Waste Management Company).

Stumm, W. & Morgan, J. J., 1996. *Aquatic Chemistry, 3rd Ed.*. New York: Wiley.

Söderlund, M., Ervänne, H., Muuri, E. & Lehto, J., 2019. The sorption of alkaline earth metals on biotite. *Geochemical Journal,* Volume 53, pp. 223-234.

Söderlund, M., Ervänne, H., Muuri, E. & Lehto, J., 2019. The sorption of alkaline earth metals on biotite. *Geochem. J.,* Volume 53, pp. 223-234.

Söderlund, M., Virkanen, J., Holgersson, S. & Lehto, j., 2016. Sorption and speciation of selenium in boreal forest soil. *J. Environ. Radioact.,* Volume 164, pp. 220-231.

Tachi, Y. et al., 2015. Matrix diffusion and sorption of Cs, Na, I and HTO in granodiorite: Laboratory-scale results and their extrapolation to the in situ conditions. *J. Contam. Hydrol.,* Volume 179, pp. 10-24.

Tsai, S.-C.et al., 2009. Cesium adsorption and distribution onto crushed granite under different physicochemical conditions. *J. Hazard. Mat.,* Volume 161, pp. 854-861.

Wissmeier, L. & Barry, D. A., 2011. Simulation tool for variably saturated flow with comprehensive geochemical raction in the two and three dimensional domains. *Env.Modell.Softw.,* Volume 26, pp. 210-218.

Yu, Q., Kandegedara, A., Xu, Y. & Rorabacher, D. B., 1997. Avoiding interferences from Good´s buffers: a contiuous series of noncomplexing tertiary amine buffers covering the entire range of pH 3-11. *Anal. Biochem.,* Volume 253, pp. 50-56.

Yu, Q., Kandegedara, A., Xu, Y. & Rorabacher, D. B., 1997. Avoiding interferences from Good´s buffers: a contiuous series of noncomplexing tertiary amine buffers covering the entire range of pH 3-11. *Anal. Biochem.*, Volume 253, pp. 50-56.

Zazzi, Å., Jakobsson, A. & Wold, S., 2012. Ni (II) sorption on natural chlorite. *Appl. Geochem.,* Volume 27, pp. 1189-1193.